NPS ARCHIVE
1964
HARTMAN, A.

SOME SELF-HEATING CHARACTERISTICS OF VERY SMALL RESISTANCE STRAIN GAGES

ANTHONY G. HARTMAN

LIBRARY
U.S. NAVAL POSTGRADUATE SCHOOL
MONTEREY, CALIFORNIA

SOME SELF-HEATING CHARACTERISTICS OF VERY SMALL RESISTANCE STRAIN GAGES

* * * * *

Anthony G. Hartman

SOME SELF-HEATING CHARACTERISTICS OF VERY SMALL RESISTANCE STRAIN GAGES

by

Anthony G. Hartman
Lieutenant, United States Navy

Submitted in partial fulfillment of
the requirements for the degree of

MASTER OF SCIENCE
IN
MECHANICAL ENGINEERING

United States Naval Postgraduate School
Monterey, California

1964

NPS ARCHIVE
1964
HARTMAN, A.

Thesis
H322

LIBRARY
U.S. NAVAL POSTGRADUATE SCHOOL
MONTEREY, CALIFORNIA

SOME SELF-HEATING CHARACTERISTICS

OF

VERY SMALL RESISTANCE STRAIN GAGES

by

Anthony G. Hartman

This work is accepted as fulfilling

the thesis requirements for the degree of

MASTER OF SCIENCE

IN

MECHANICAL ENGINEERING

from the

United States Naval Postgraduate School

ABSTRACT

The self-heating of small foil resistance strain gages is studied both analytically and experimentally. The thermal resistance of the strain gage-specimen combination is obtained and utilized in relating the steady state temperature rise of the gage grid to the magnitude of the electrical current flowing through the gage. It is shown that the primary mechanism for dissipation of the gage self-heat is conduction through the gage backing, bonding adhesive, and specimen, then radiation and convection from the specimen surfaces to the environment. The heat dissipation paths provided by the lead wires and the exposed gage grid and tab surfaces are found to account for a negligible fraction of the heat transferred. For the smallest gages the backing and adhesive contribute nearly all of the thermal resistance of the primary path. In the latter cases it is shown that gage heating is substantially independent of the thermal conductivity or size of the specimen and that the gage power dissipation per unit grid area is the dominant parameter in predicting the steady-state temperature rise of the grid.

ACKNOWLEDGMENT

The author wishes to express his gratitude to Dr. Robert E. Newton in appreciation for arousing his interest in the subject matter leading to the selection of this topic and for the guidance and encouragement he provided throughout the course of this investigation.

TABLE OF CONTENTS

Section	Title	Page
1.	Introduction	1
2.	Fundamental Hypothesis	3
3.	Experimental Procedures and Equipment	17
4.	Discussion of Results	31
5.	Conclusions	43
6.	Bibliography	44
Appendix		
I.	Development of Thermal Resistance Parameters	I-1
II.	Calculation of Combined Thermal Resistance of System	II-1
III.	Experimental Results	III-1

LIST OF TABLES

Table	Title	Page
II-1	Strain Gage Data	II-2
II-2	Resistance to Heat Flow from Exposed Surface of Gage Tab	II-6
II-3	Resistance to Heat Flow from Exposed Surface of Gage Grid	II-6
II-4	Thermal Resistance of Small Hemisphere under Grid	II-11
II-5	Resistance to Heat Flow through Hollow Hemisphere Portion of Specimen	II-12
II-6	Equivalent Combined Resistance of R_{hb}, R_{fk}, R_e, and R_{fh}	II-14
II-7	Thermal Resistance of Specimen under Gage Grid	II-16
II-8	Combined Thermal Resistance of Entire Heat Transfer System	II-22
III-1	Fractional Resistance Change of Gage at Uniform Elevated Temperature	III-6
III-2	Thermocouple Temperature Rise at Various Gage Power Levels	III-7
III-3	Fractional Resistance Change at Various Gage Power Levels	III-8

1. Introduction

The usefulness of resistance strain gages is dependent upon the accurate measurement of resistance changes due to changes in external loading. In practice, however, the measured change in resistance is not always entirely attributable to the load change since the resistivity of the gage material is dependent upon temperature. Strain gage resistance also varies with the temperature dependent elongations of both the gage and the specimen to which it is attached. A great deal of study in the strain gage field has been concerned with the effects of elevated environmental temperatures on gage performance and methods by which these effects may be compensated or eliminated /12; 13; 24; 27; 28;29; 34; 37; 42; 45; 48/.* But, in most investigations to date, the effect of self-heating by the I^2R losses of the gage has been either neglected or described in general terms.

Since foil gages were introduced into the resistance strain gage field the size of these devices has been greatly reduced. Miniature foil gages are presently available with gage lengths as small as 0.015". Because of the very small area available for dissipation of the Joulean heat in these miniature gages the apparent strain due to the self-heating effect has become an even more appreciable part of the gage output than

*Bibliographic references are shown as /1-1,2; 2/. This example would indicate reference #1, pages 1 and 2 and reference #2 in the Bibliography beginning on page 44 .

that for the larger foil and wire gages. In some applications this effect might be the limiting factor on gage utility since the sensitivity of the strain indicator is directly proportional to the gage current /25; 42/ while the amount of heat generated is proportional to the square of the gage current (I^2R).

This study was undertaken, then, in an attempt to determine some of the self-heating effects on the performance of very small foil gages. A more specific goal of this study was to obtain a rational expression relating the steady-state gage grid temperature and the thermal power dissipated by the gage. The analytical treatment of the problem involves a theoretical heat transfer analysis leading to an expression for the thermal resistance of the gage-specimen system. The validity of the theoretical predictions concerning gage performance is then determined experimentally. Because of the many variables involved in strain gage technology the experimental investigation was restricted to determining the effect of several values of gage current on small foil gages of the same type, but of different dimensions, attached with the same bonding adhesive to flat plates of stainless steel and aluminum of various sizes.

2. Fundamental Hypothesis

In order that a resistance strain gage may accomplish its designed function an electrical current must flow through it. But, when the current flows through this region of relatively high resistance some of the electrical energy provided becomes "lost" to the electrical circuit. This "lost" electrical energy manifests itself as heat and must be removed from the immediate vicinity of the strain gage to prevent excessive grid temperatures which enhance the occurrence of the undesirable effects described below. The self-heating problem in these gages, then, is primarily concerned with the amount of heat generated and the means by which it may be dissipated.

The thermal power developed by an electrical resistor is

$$q_o = I_g^2 R_g \,. \tag{1}$$

For application to the case at hand, q_o is the heat generated per unit time by the electrical current flowing through the gage, I_g is the electric current flowing, and R_g is the electrical resistance of the gage.

As an example, if a current of 50 milliamps flows through a 120 ohm gage the heat generated is only 0.300 watt or 1.024 BTU/hr. However, as shown below, almost all of the heat generated per unit time is dissipated from one face of the gage grid under steady state conditions. Considering the total grid area for a gage having grid dimensions of 0.015" x 0.020" this

small amount of heat results in a heat flux of about 490,000 BTU/hr-ft^2. For purposes of comparison, the maximum heat flux in the seed elements of the Shippingport Thermal Nuclear Power Reactor is 418,000 BTU/hr-ft^2 / 6-587/. Since the local temperature rise above a given datum is directly proportional to the heat flux there will be an appreciable temperature rise at the gage grid in the above example.

Scott /45-80/ divides the effects of this temperature rise into three stages. In the first stage, small temperature increases result in apparent strain indication because of the temperature coefficient of resistance effects as described below. This stage is characterized by a near-linear relationship between apparent strain and the power dissipated by the gage. Further increases in gage current (and hence temperature) cause the gage bond to be weakened and lower the sensitivity of the gage to strain changes in the specimen. In this second stage the relationship between apparent strain and temperature becomes non-linear. Increasing the current further still increases the departure from linearity and eventually results in destruction of the gage. This is the third stage.

For reliable strain indications, then, it is desirable to know the apparent strain for a given gage current. This may be obtained in three steps for the range of first stage temperature effects (the normal operating range for most applications). First, the temperature of the gage must be determined as a function of gage current such that

$$\Delta \overline{T}_o = q_o R_{th} \tag{2}$$

where: $\Delta \overline{T}_o$ is the average temperature rise of the gage grid above the ambient temperature of the environment,

R_{th} is the equivalent thermal resistance of the gage-specimen system, and

q_o is as previously defined.

Then, combining (1) and (2),

$$\Delta \overline{T}_o = I_g^2 R_g R_{th} \quad . \tag{3}$$

Second, the fractional resistance change as a function of temperature is obtained. This expression may be written as

$$\frac{\Delta R_g}{R_g} = \eta \Delta \overline{T}_o = I_g^2 R_g R_{th} \tag{4}$$

where η is defined as the temperature coefficient of electrical resistance of the strain gage system. Finally, the expression for strain as a function of fractional resistance change,

$$\epsilon_a = \frac{1}{F} \frac{\Delta R_g}{R_g} \quad , \tag{5}$$

is used to determine the apparent strain ϵ_a, where F is the gage factor supplied by the manufacturer for the gage. Combining (4) and (5)

$$\epsilon_a = \frac{1}{F} (\eta I_g^2 R_g R_{th}), \tag{6}$$

which is the desired relationship.

Calculations of apparent strain will not be made in this study but are easily obtained from Eq. (6) provided that the parameters indicated are known. For any gage installation the gage factor and gage resistance are provided by the manufacturer. The gage current may be easily obtained from measurements. However, the temperature coefficient of electrical resistance and the equivalent thermal resistance of the system must be derived.

For environmental temperature changes it may be shown /45-86/ that the temperature coefficient of resistance for the system is

$$\eta' = \beta - \alpha + f(\alpha_p - \alpha) \qquad (7)$$

where: β is the temperature coefficient of resistivity for the gage material,

α is the coefficient of thermal expansion for the gage material,

α_p is the coefficient of thermal expansion for the specimen material, and

f is the strain sensitivity of the gage material /48-II.22.29/.

This expression was developed originally for wire gages but also may be applied to foil gages.

If the gage is self-temperature-compensated for a given type of specimen material then (7) becomes

$$\eta' = \beta - \alpha + f(\alpha_c - \alpha) = 0 \qquad (8)$$

where α_c is the thermal coefficient of expansion of the material for which the gage is compensated. Then, in general, for the self-temperature-compensated gages on different materials, subtracting (8) from (7),

$$\eta' = f(\alpha_p - \alpha_c) \tag{9}$$

which is the result shown by Higson /28-159/.

Combining the work of Stein /48-I.6/ and Perry and Lissner /42-158,159/ it may be shown that

$$f = \frac{F(1 + k)}{1 - \mu_c k} \tag{10}$$

where: k is the transverse sensitivity ratio of the gage grid,

μ_c is Poisson's ratio for the compensated specimen material, and

f and F are as defined above.

The transverse sensitivity ratio, k, is extremely small for these small foil gages because the end loops which join adjacent grid filaments are much larger than the filaments themselves /1-4;5-3/. Considering the order of the approximations to be employed in the heat transfer analysis, it may be assumed that the transverse sensitivity in (10) is negligible and

$$f = F . \tag{11}$$

For the case of self-heating, however, Eqs. (7), (8), and (9) do not strictly apply because the temperature rise at the gage grid is greater than the rise at the surface on which the strain is being measured. In addition, the temperature rise

at the specimen surface is confined to a very small region. Since all of the specimen material except this minute region is at an appreciably lower temperature it will act as a physical constraint on the higher temperature region resulting in a practically negligible thermal expansion of the region. Hence, the thermal strain in this region ($\alpha_p \Delta T$) is assumed to be negligible and the temperature coefficient of resistance of the system for the case of self heating may be written, from (9) and (11),

$$\eta = -F\alpha_c \,. \tag{12}$$

The equivalent thermal resistance of the system, R_{th}, used in Eq. (6) is most difficult to obtain. The determination of its magnitude requires a steady-state heat transfer analysis of the entire strain gage-specimen complex. This parameter is the major topic of the remainder of this study.

To begin this heat transfer problem it may be observed in Figure 1 that, basically, there are three paths by which the Joulean heat may be removed and dissipated. These are: (1) by conduction through the gage backing, the bonding adhesive and the specimen to which the gage is attached; (2) by conduction through the gage covering (if there is any) and then by radiation and convection from the exposed surface; and (3) by conduction, radiation and convection from the terminal tabs and leads. The latter is actually composed of two paths since there is a tab at each end of the gage. This system, in steady state, is shown schematically in Figure 2 for a three-

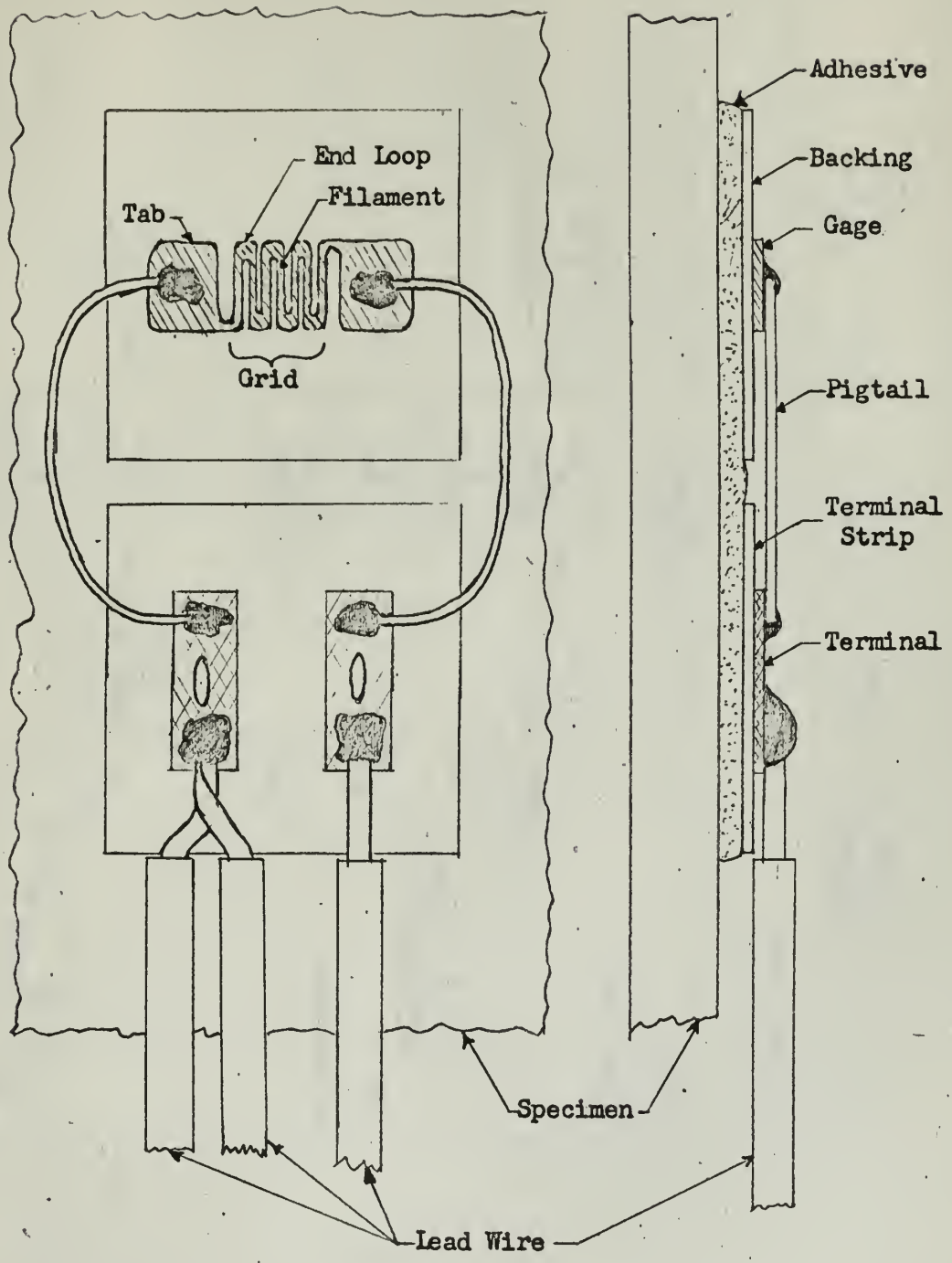

Figure 1

Gage Installation

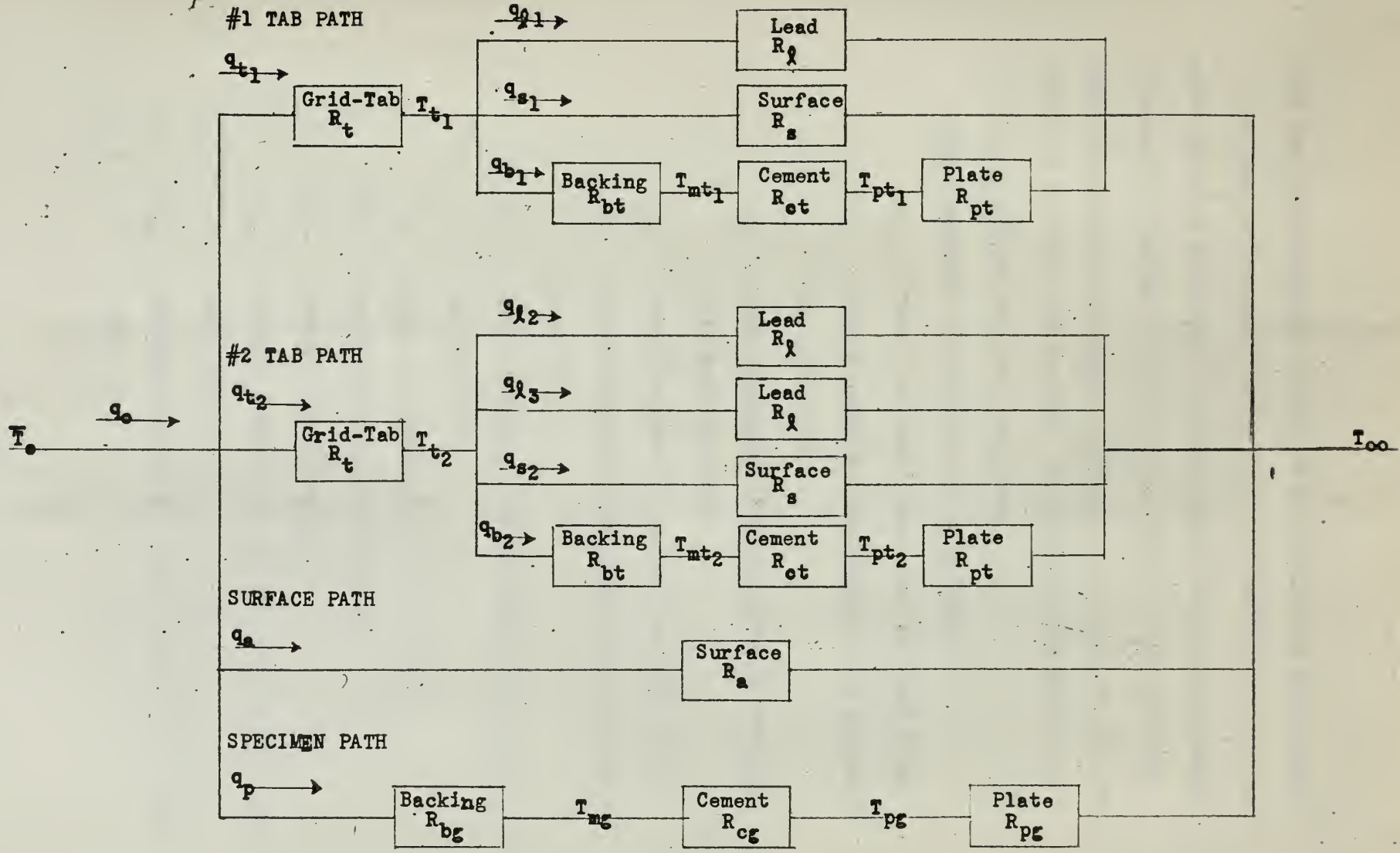

FIGURE .2

Schematic Diagram of Steady State Heat Transfer System

lead gage installation. It may be noted from the figure that if the gage is connected by the usual two-lead method both tab paths would be identical. In that case it would be necessary to show only one path on the diagram with the understanding that its equivalent thermal resistance is one half of that for either of the individual paths. The pigtails and terminals will be considered with the lead wires.

The nomenclature of Figure 2 is as follows:

q_t	heat dissipated from a tab per unit time
q_a	heat dissipated from exposed grid surface per unit time
q_p	heat dissipated through specimen from gage grid per unit time
q_ℓ	heat dissipated by a lead per unit time
q_s	heat dissipated from exposed tab surface per unit time
q_b	heat dissipated through specimen from gage tab per unit time
T_∞	ambient temperature of environment
$\overline{T}_o$	average gage grid temperature
T_t	average tab temperature
T_{mg}	average temperature between backing and cement under grid
T_{mt}	average temperature between backing and cement under tab

T_{pg} average temperature between cement and specimen under grid

T_{pt} average temperature between cement and specimen under tab

R_{bg} resistance to heat flow through gage backing under grid

R_{cg} resistance to heat flow through adhesive under grid

R_{pg} resistance to heat flow through specimen and its surfaces under grid

R_a resistance to heat flow from exposed surface of gage grid

R_t resistance to heat flow from gage grid to tab

R_{bt} resistance to heat flow through gage backing under tab

R_{ct} resistance to heat flow through adhesive under tab

R_{pt} resistance to heat flow through specimen and its surfaces under tab

R_s resistance to heat flow from exposed surface of gage tab

R resistance to heat flow through a lead wire

Considering this schematic diagram as an electrical analogue of the steady state heat transfer mechanism, basic electrical circuit analysis /38;35/ will permit calculation of the gage temperature for a given gage current by Eq. (3) provided the ambient temperature and all of the thermal resistances shown are known.

Determination of the various thermal resistance parameters by the methods of rigorous heat transfer theory /11;16;19;21;22;31;33;43;44;46;49/ and then combining them to form R_{th} would indeed be most complex and quite formidable. Since one of the objectives of this study was to attempt to develop relatively simple, rational expressions for the behavior of the system a less complex approach was devised.

The individual thermal resistance parameters were developed by means of linear heat transfer theory and appropriate approximations in Appendix I. The associated assumptions and resulting restrictions were included for each parameter obtained.

Normal procedure would then be to combine these resistances in parametric form by circuit analysis methods to arrive at the equivalent thermal resistance of the system. As can be readily imagined, the algebra involved in performing this task for the circuit of Figure 2 with the resistance parameters developed in Appendix I would become quite involved.

Alternatively, the individual thermal resistances were evaluated in Appendix II using relevant physical properties and dimensions for the system components. From the relative magnitudes obtained for the resistance parameters and their respective locations in the circuit it was observed that most paths transmit a negligible fraction of the heat. In particular, it was shown that the lead wires have a negligible effect on the heat transfer mechanism and that the only path by which any

appreciable amount of heat is dissipated to the atmosphere is through the specimen. Thus, based on the results of Appendix II, the equivalent thermal circuit of Figure 2 was reduced to that of Figure 3 and the equivalent thermal resistance of the entire system is

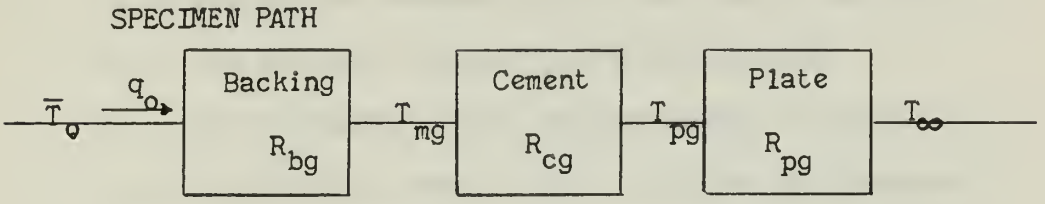

Figure 3.
Reduced Schematic Diagram of
Steady State Heat Transfer System

$$R_{th} = R_{bg} + R_{cg} + R_{pg}$$

$$= \frac{1}{A_g}\left[\frac{d_b}{k_b} + \frac{d_a}{k_a}\right] + \frac{2t - \sqrt{A_g/\pi}}{2 k_p t \sqrt{\pi A_g}}$$

$$+ \frac{\ln \frac{r_p}{\sqrt{2/3}\, t} + \frac{k_p}{h r_p}}{2\pi h\left[\frac{k_p}{h}(r_p + t) + \frac{r_p^2}{2} - \frac{t^2}{3}\left(1 + \ln \frac{r_p}{\sqrt{2/3}\, t} + \frac{k_p}{h r_p}\right)\right]} \qquad (13)$$

The parameters employed in Eq. (13), as defined in Appendices I and II, are:

A_g the total surface area covered by the gage grid

d_b the thickness of the gage backing

d_a the thickness of the bonding adhesive

k_b the thermal conductivity of the backing material

k_a the thermal conductivity of the adhesive

t the thickness of the specimen under the gage

k_p the thermal conductivity of the specimen material

r_p the equivalent radius of the specimen surface

h the surface coefficient of heat transfer

Examination of the calculated values for R_{th} listed in Table II-8 (p. II-22) shows that the overall thermal resistance has relatively little dependence on the specimen size except for the gage with 3.9×10^{-3} in^2 grid area where, as will be seen below, the self-heating effect is much less significant than for the smaller gages. The tabulated values also indicate that the variation with specimen material between the highly conductive aluminum and the poorly conducting stainless steel is less than 10% for the smallest gage and only about 20% for the largest of the three gages. It is quite evident, however, that the greatest variation is due to the gage size and its effect on the resistance of the backing and adhesive.

Based on these results it is hypothesized that for the smallest gages (those with grid areas of less than 0.001 square inches) the specimen dependence can be eliminated from Eq. (13). For

these extremely small gages, then, the equivalent thermal resistance of the system becomes

$$R_{th} = \frac{1}{A_g} \left[\frac{d_b}{k_b} + \frac{d_a}{k_a} \right] . \qquad (14)$$

Having obtained an expression for R_{th}, the average gage grid temperature for a given gage current may now be obtained from Eq. (3):

$$\overline{T}_o = T_\infty + I_g^2 R_g R_{th} . \qquad (15)$$

For the general case R_{th} may be calculated from (13). For those installations utilizing extremely small gages the thermal resistance may be approximated by (14) and the grid temperature rise becomes

$$\Delta \overline{T}_o = \frac{I_g^2 R_g}{A_g} \left[\frac{d_b}{k_b} + \frac{d_a}{k_a} \right] . \qquad (16)$$

As stated by Stein /47/ and others, the performance of a strain gage installation is only as good as the quality of the bond between the gage and the specimen. It has been tacitly assumed in the preceding derivation of R_{th} that the gage is perfectly bonded to the specimen. If, for a given installation, a good quality bond is not assured the performance of the system would be highly unpredictable.

3. Experimental Procedures and Equipment

The primary objective in conducting these tests was to verify the validity of the expression for the equivalent thermal resistance of the system, Eq.(13). It is generally accepted /34-448; 1-8/ that the material and size of the specimen are limiting factors on the operating power level of the gage. The theoretical results of Section 2 indicate that these variables have a relatively minor effect on the heat transfer mechanism of the system. More specifically, then, these tests were performed to determine the effects of the specimen size and material on heat dissipation. In addition, tests were made to determine the validity of the approximations leading to the reduced thermal circuit of Figure 3. These were the negligibility of lead wire effects and that of heat dissipation from tabs and exposed grid surfaces. Further tests were made to verify the effects of gage size on the combined thermal resistance and to determine the extent of the linear range of fractional resistance change with power level.

The gages used for these tests were temperature compensated for stainless steel and are described in detail in Appendix II-A (p. II-1). They were bonded to square, flat plates of stainless steel in the 300 series and 2024 aluminum alloy at the approximate center of the plate surface with Eastman 910 adhesive. The installation procedure prescribed by Bean /10/ and Perry and Lissner /42-43/ employing cellophane tape and the "wallpaper

hanging" technique was used to attach the gages and terminal strips. However, thumb pressure was applied for two minutes instead of the specified one minute because of a failure in one of the early applications.

Leads were attached using Bean's "Tape Masking System" /10/. In the early tests AWG #22, solid, copper wire with vinyl insulation was used for the leads. A single strand of 22 gage stranded wire was used for the pigtail extending from the terminal strip to the gage tab. These leads were found to be very stiff and cumbersome and after a few terminal strips and gage tabs were pulled off a change was made. In all of the later tests AWG #28, stranded, copper wire was employed for connecting the gages and a single strand of this wire was used for the pigtail. The lead size used in each test is tabulated with the results of that test in Appendix III.

As previously stated, one of the prerequisites for obtaining meaningful results is the assurance of a good adhesive bond between the gage and the specimen. Following the recommendations of the Eastman Kodak Company /2-2/ and Stein /48-II.23.40/ the gage-specimen systems were "baked out" in order to try to establish uniformity among the various installations. A Cenco-DeKhotinsky Constant Temperature oven was used. Temperatures were cycled to approximately 165°F at a rate of from four to eight hours per cycle. Several temperature cycles were made for each installation to accelerate curing, increase the bond strength and minimize thermal hysteresis. The number of temperature cycles prior to

each test is tabulated with the results. Electrical resistance versus temperature data were taken for a number of these cycles and are presented in both tabular (p. III-6) and graphical (p. 32) form.

Two methods of experimental verification of the equivalent thermal resistance of the system were attempted: directly by temperature measurement and indirectly by resistance measurements. The same basic equipment arrangement was used for both methods.

The test plate was supported, gage side up, by wooden dowels at each corner. The dowels, set into tight fitting holes in a base board, held the plate about eight inches above the board. This allowed sufficient space for natural convection from the bottom of the plate.

An Ellis Associates' Bridge Amplifier Meter, Model BAM-1 /3;42-85/ was used to provide the basic Wheatstone bridge circuit, power supply and indicator. This instrument was selected primarily for its capability to provide steady bridge voltage at variable levels with the simplest of controls, a potentiometer. It may be used with gage currents up to 50 milliamps by adding batteries at external terminals. The bridge voltage may also be measured at external terminals. These features made it particularly suitable for controlling gage current over a wide range.

All tests were made with the power switch of the BAM-1 set at "2". This eliminated a 120 ohm internal resistor in series with the batteries and provided for connection of two external

gages. Rather than use a dummy gage which would compensate for the temperature effects in the test gage, a General Radio Decade Resistor, type #1432-M, was used at a setting of 120 ohms. This is a high quality device and, according to the manufacturer, may be used as a laboratory standard for currents up to 80 milliamps at 120 ohms. This limit is well above the current excursions in these experiments.

The applied bridge voltage, V_b, was measured at terminals A and B on the BAM-1 using a Weston d-c voltmeter, Model 931. Voltages were read on the 0-15 volt scale except for the runs to detect non-linearities. For the latter cases the applied voltage range was extended to obtain higher gage currents and the required higher voltages were read on the 0-150 volt scale with a corresponding loss of accuracy. Since the BAM-1 contains only 12 volt bridge supply batteries, they were supplemented by the series addition of external batteries when the gage test currents so required. When an additional battery was inserted the circuit remained the same except that the gage connection was moved from terminal B on the BAM-1 panel, where the negative terminal of the external battery was now connected, to the positive terminal of the external battery, B'. (See Figure 4, p. 27)

The test gages were connected to the BAM-1 and the decade box by the three-wire method /42-71; 24-1167; 39-47/, for most of the runs. This system was employed to compensate for any resistance changes due to temperature variations in the lead wires. In this manner, the observed temperature effects were

restricted to those considered in the theoretical analysis of Section 2. For determining the lead wire thermal effects the test gage was connected in the standard two-wire bridge arrangement.

The direct method for thermal resistance verification is based on Eq. (3), from which

$$R_{th} = \Delta \bar{T}_o \; / \; I_g^2 \, R_g \quad . \tag{17}$$

That is, the equivalent thermal resistance of the system is equal to the average temperature rise of the gage grid per unit power dissipated from the gage. Hence, the desired thermal resistance may be obtained for a given gage and operating level from measurements of the grid and environmental temperatures. Because of possible inaccuracies in measuring the required parameters, the thermal resistance would, in practice, be determined as the average slope from a plot of the grid temperature rise versus gage power level for various values of gage current. The temperature of the atmosphere in the vicinity of the test apparatus was measured with a laboratory grade mercury thermometer, Cenco #19235-A. Determination of the grid temperature proved to be most difficult.

It was expected that a measurement of the temperature at the approximate center of the exposed grid surface would yield a value somewhere between the average and the maximum grid temperature. Using this measured value in Eq. (17) with the corresponding gage current and electrical resistance would provide sufficiently accurate values for the thermal resistance of the system.

Baker /8-II.170/ states that, "Unfortunately, the procedure of measuring temperatures at interior points and extrapolating to the surface is almost the only unequivocal method for the measurement of surface temperatures, and it is not always possible to apply this method." It is definitely impossible to apply this method to the thin foil of the grid and quite impractical to use it at any other location where a significant temperature rise exists without completely disrupting the heat transfer mechanism of the ordinary gage installation. Some portable surface-contact thermocouples /8-II.176/ are commercially available but these are either surface piercing types or cover too large an area and are not considered feasible for use in this case. This surface temperature measurement is further complicated by the fact that the temperature measuring device must be electrically insulated from the surface so as not to alter the current flow through the grid.

In spite of the complications described above, it was decided to attempt to measure the surface temperature of the grid by thermocouple techniques. A basic, two junction thermocouple circuit /7-15/ was set up with the reference junction immersed in an ice bath. A Leeds and Northrup #776494 null-detecting potentiometer was used as the indicating instrument.

Two different detecting junctions were tried. The first was composed of 0.010" diameter iron and constantan thermocouple wires. These were butt-welded together to form the junction

using a Micro Products, Model J-E-S automatic micro-weld butt welder /7-49/. The second was a Baldwin-Lima-Hamilton, Micro-Miniature Thermocouple, Type TCC-ES-50, possessing a beaded junction /7-42/ of 0.001" diameter copper and constantan wires.

For all of the temperature-recording runs, except one, the detecting junctions were coated with a thin film of varnish of the type used as insulation on electric motor windings. This was accomplished by dipping the junction into the varnish and allowing the excess to run off. Drying was completed at room temperature after 24 hours. The one exception was an iron-constantan junction to which Sauereisen Low Expansion Cement #29 was applied in paste form and allowed to dry at room temperature for 24 hours. This cement is claimed by the manufacturer to be an excellent heat conductor and to exhibit high electrical resistance. By these means the thermocouple junctions were electrically insulated in order that the electrical gage circuit would not be affected when the thermocouple was placed in contact with the grid surface.

In all of the iron-constantan junction installations the thermocouple circuits were completed with the junction wires since the lengths of the leads were short and, in this manner, intermediate junctions with other materials (e.g., copper) were avoided. For two of the cases where the micro-miniature thermocouples were used the interconnecting leads were 0.020" diameter copper and constantan wires. The remainder of the micro-miniature juntion installations utilized 0.010" diameter copper and

constantan leads. A discussion of "Heat Transfer to the Ambient Via the Leads" is given by Baker /8-I.71/. His analysis results in an expression for the heat transferred to the atmosphere by the leads per unit time comparable to Eq. (I-16) (p.I-5). But, in Appendix I, this expression was the basis for obtaining the thermal resistance of the leads, Eq. (I-17). Using (I-17) it was found that the iron-constantan pair of 0.010" diameter had a thermal resistance of 1640°F per BTU/hr. Similarly, the copper-constantan pair of 0.001" diameter in the micro-miniature thermocouple provided a resistance to heat flow of 32,600°F per BTU/hr. In the latter case, about one inch of these wires is sufficient to be considered "infinitely long" in the thermal sense. Hence, the micro-miniature thermocouples should provide the more accurate data because of their high resistance to heat flow.

For one run an iron-constantan thermocouple was taped to the plate with the junction in position on the grid. The entire plate surface was then covered by a plastic foam pad three inches thick. Another test plate of the same size was placed on top of the pad to press the thermocouple against the gage grid. In the remainder of the runs utilizing iron-constantan junctions the thermocouple leads were clamped vertically between rubber strips in a test tube clamp mounted on a laboratory ring stand about three inches above the detecting junction. The clamp was lowered on the stand until the junction was in contact with the grid surface. Lowering was continued until a bow of one-half to one

inch was observed in the leads. The junction was then centered on the grid as accurately as visual observation through a magnifying glass would allow.

The micro-miniature thermocouples were all mounted in the same manner. In these devices, the junction protrudes an extremely short distance beyond the end of a very small diameter stainless steel tube which houses the 0.001" wires. Above the tube the junction wires are attached to 0.010" pigtails of the same material. The pigtail connections and the upper part of the tube are then encased in a larger cylinder of ceramic material with the pigtails extending from the top surface. The ceramic cylinder was clamped vertically in a lucite block which was attached to the horizontal arm of a dial indicator stand. The junction was then lowered into position on the grid by the lead screw action of the arm to the point where perceptible bending of the junction wires could be observed through the magnifying glass.

An additional problem, common to all of these thermocouple installations, is that of thermal resistance at the contact between the junction and the grid. This subject is treated by Baker /8-I.74/. He states that the coefficient for surface boundary conductance over the contact area has been observed to vary from 150 to 15,000 BTU/hr-ft^2-°F depending on the materials involved, the contact pressure, the smoothness of the contact surfaces and the temperature. Because of the wide range of this coefficient the possibility of determining an analytical correction for the measured temperature to account for this thermal

contact resistance appeared very remote. However, it was expected that careful scrutiny of the experimental data coupled with an approximate heat transfer analysis might result in a reasonable estimate for the correction.

Another means of measuring grid temperature which would not involve physical contact with the strain gage is that involving infrared techniques /17;23;26;41/. Infrared radiometers and pyrometers have been developed to measure temperatures of about 25°C and above. Ovrebo discusses these instruments /41-1636/ and lists some of their present applications. These techniques appear as if they might be well adapted to this temperature measuring problem. However, further discussion of infrared temperature measurement is beyond the scope of this study.

It may be observed from the preceding discussion that the temperature measuring method of thermal resistance verification is not as "direct" as the theory predicts it to be when the encumbrances of experimental technique are considered. Because of these complexities, a second method of verification was attempted involving measurements of the electrical resistance changes of the gage due to the self-heating. The basis for this approach is Eq. (4) which may be rewritten as

$$\frac{\Delta R_g / R_g}{I_g^2 R_g} = \eta R_{th} . \qquad (18)$$

That is, the fractional resistance change of the strain gage is equal to the temperature coefficient of resistance of the gage-specimen system times the equivalent thermal resistance of the system.

The relationship between the numerator and denominator of the term on the left in (18) was shown by Campbell /15/ to be nearly linear for first stage self-heating effects in wire gages. The theory developed in Section 2 shows that both η and R_{th} are constants for a given gage installation. Therefore, it is anticipated that the slope of a plot of the fractional resistance change versus the gage power output would be nearly constant and equal to the product of η and R_{th} calculated from Eqs. (12) and (13) respectively.

The only equipment required for this resistance approach is that which has been previously described as being common to both methods (p. 19). A schematic diagram of the strain gage test circuit for the three-lead gage connection with external batteries is shown in Figure 4. The resistance values for the

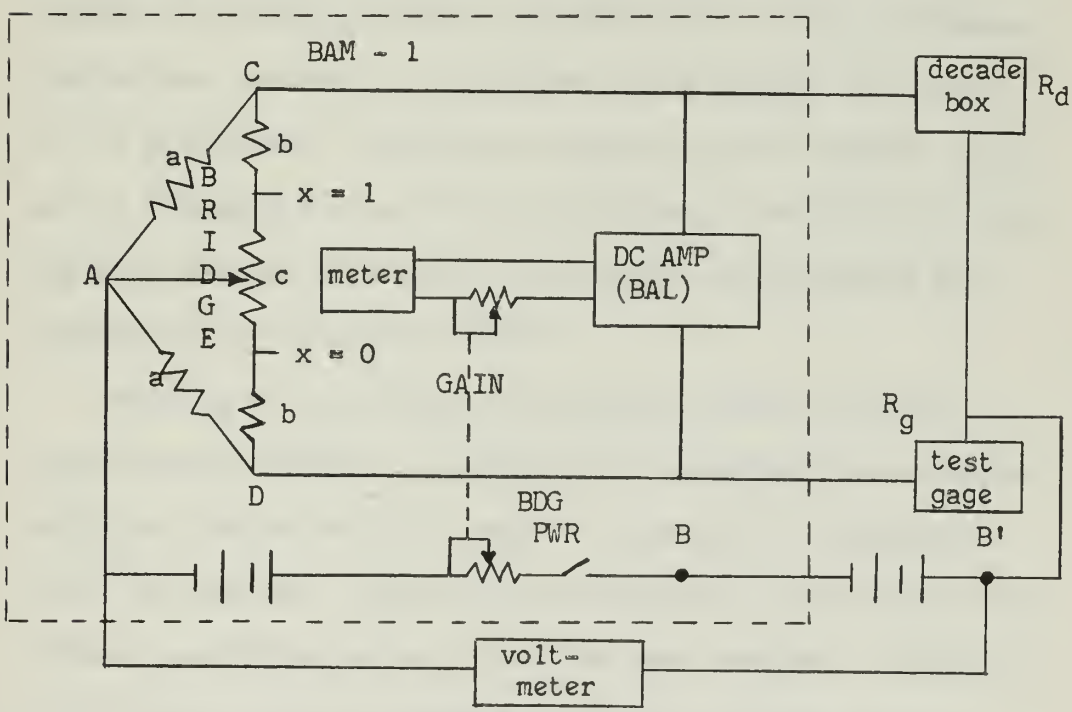

Figure 4
Strain Gage Test Circuit

circuit elements are:

a = 402 ohms,

b = 10,000 ohms,

c = 200,000 ohms,

R_d = 120 ohms, and

R_g = 120 ohms.

The value of the applied bridge voltage was calculated from basic balanced bridge circuit theory using the equation given by the manufacturer /3-7/ for each gage current level desired. This value, V_b, was set on the voltmeter by means of the gain control. The amplifier was balanced to obtain a zero meter reading with the "BDG PWR" switch in the open position. After closing the switch the bridge was balanced by adjusting the "BRIDGE" potentiometer, c, until the meter indicated zero. The potentiometer reading was recorded to four places as the decimal fraction, x, of its resistance. The relative position of the "BRIDGE" wiper arm is indicated on the circuit of Figure 4. The bridge voltage was held constant by monitoring the voltmeter and making minor adjustments with the gain control.

Readings of the relative potentiometer wiper position, x, versus bridge voltage, V_b, obtained in this manner were recorded every ten minutes until at least two consecutive readings provided the same data. When this was achieved it was assumed that thermal equilibrium of the system had been attained. The wiper position data were then reduced to values of $\Delta R_g/R_g$ by the

method described below and plotted as a function of $I_g^2 R_g$. The average slopes of the resulting curves were then determined, divided by η and compared with the calculated value of R_{th} for the corresponding cases in accordance with Eq. (18). The values of $\Delta R_g/R_g$, $I_g^2 R_g$ and the experimental thermal resistances as well as the calculated R_{th}'s are tabulated in Appendix III. The plotted results for significant cases are also presented in Section 4.

It is to be noted that the BAM-1 was designed primarily for use as a deflection type indicator rather than a null indicator as employed in these tests. When used as a deflection type indicator the meter may be calibrated to read the fractional resistance change directly. However, the gain setting must remain unchanged throughout the test run. Since, in these experiments, the gain control was used to vary the gage current, the null method had to be used.

An analysis of the bridge circuit of Figure 4 under balanced conditions as employed in the null detection method shows that the fractional resistance change may be expressed as

$$\frac{\Delta R_g}{R_g} = \frac{R_d}{R_g} \left[\frac{(P-b)\, xc + Pb - (xc)^2}{(M-N)\, xc + MN - (xc)^2} \right] - 1 \qquad (19)$$

where: $M = b + c = 210{,}000$ ohms,

$N = a + b = 10{,}402$ ohms,

$M - N = 199{,}598$ ohms,

$P = a + b + c = 210{,}402$ ohms,

$MN = 2{,}184{,}420{,}000$ ohms^2,

$P - b = 200{,}402$ ohms,

P_b = 2,104,020,000 ohms^2 and,

x = fractional potentiometer dial reading.

If the nominal resistance of the gage is used, $R_d / R_g = 1$. Since the actual value of R_g may differ slightly from the nominal value due to manufacturing tolerances this ratio was arbitrarily set to yield zero resistance change for a gage current of two milliamps in each test run. The values of $\Delta R_g / R_g$ tabulated and plotted in Appendix III were calculated from Eq. (19) under this premise.

The second method of thermal resistance verification involving electrical resistance measurements, although theoretically less direct than the temperature measuring method, is seen to be much more direct in practice even though the data reduction scheme might appear somewhat tedious. This approach was selected for thermal resistance verification after it was found that the temperature measuring scheme did not provide meaningful results.

4. Discussion of Results

Following the procedures of Section 3 many tests were performed in an attempt to verify the analytical conclusions of Section 2 and, in so doing, to confirm the validity of the approximations which led to those conclusions. The experimental results and some of the more specific details of the tests involved are presented in Appendix III. Some of the test results are given in graphical form in this section. These curves were plotted from typical experimental results selected to demonstrate the effect of particular influences on gage performance. A discussion of these curves including correlation between the predicted and experimental effects of the system variables will be found in the ensuing paragraphs.

The fractional changes in electrical resistance of the gage due to elevated oven temperatures for several of the uniform heating cycles are listed in Table III-1 (p. III-6). A graphical presentation of the results from three of these temperature cycles is given in Figure 5 (p. 32). Comparison of the first and third cycle curves for gage 1A* on stainless steel shows the necessity for thermal cycling to obtain the desired temperature compensation. The theoretical temperature coefficient of resistance for gages operating under these conditions is shown to equal zero in Appendix III (p. III-1). Except for minor

*The letters following the gage numbers indicate different gages of the same numbered type.

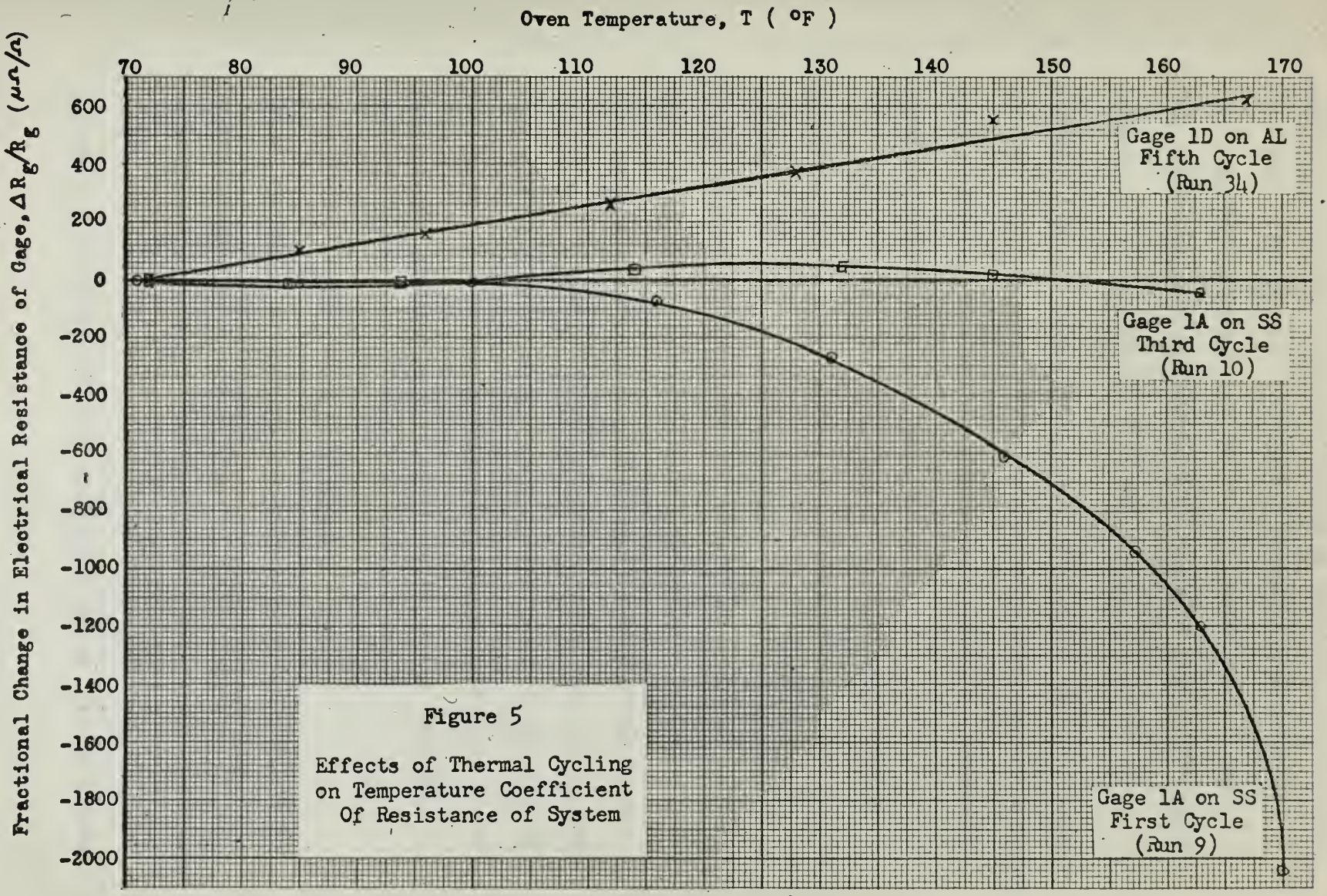

Figure 5

Effects of Thermal Cycling on Temperature Coefficient Of Resistance of System

oscillations this is shown to be true by the third cycle curve. The third curve plotted in Figure 4 indicates the resistance variation with temperature for the fifth heat cycle of gage 1D attached to an aluminum plate. This curve is seen to be nearly linear with a slope of 6.6 $\frac{\mu\Omega}{\Omega}$ per ^{o}F. As determined in Appendix III, the predicted slope is about 6 $\frac{\mu\Omega}{\Omega}$ per ^{o}F. These curves, then, show that the analytical expression for the temperature coefficient of electrical resistance provides a reasonably accurate prediction of its magnitude.

Figure 6 shows the variation of the temperature rise at the thermocouple as a function of the power dissipation level of the gage for several of the attempts at verification of the system thermal resistance by the temperature measuring method. These tests are discussed in detail in Appendix III. The results from which the curves were plotted are listed in Table III-2 (p. III-7). It may be observed from the figure that the temperature rise becomes non-linear as the power level of the gage is increased. This effect is attributed to the temperature dependence of the physical properties of the materials involved. From Eq. (17)

$$R_{th} = \Delta\bar{T}_o / I_g^2 R_g .$$

Hence, the slope of these curves would represent the equivalent thermal resistance of the system if the measured temperature rise was actually that of the gage grid. The slope of the linear portion of each of the curves plotted was determined and listed in Table III-2 along with the analytical values for the system

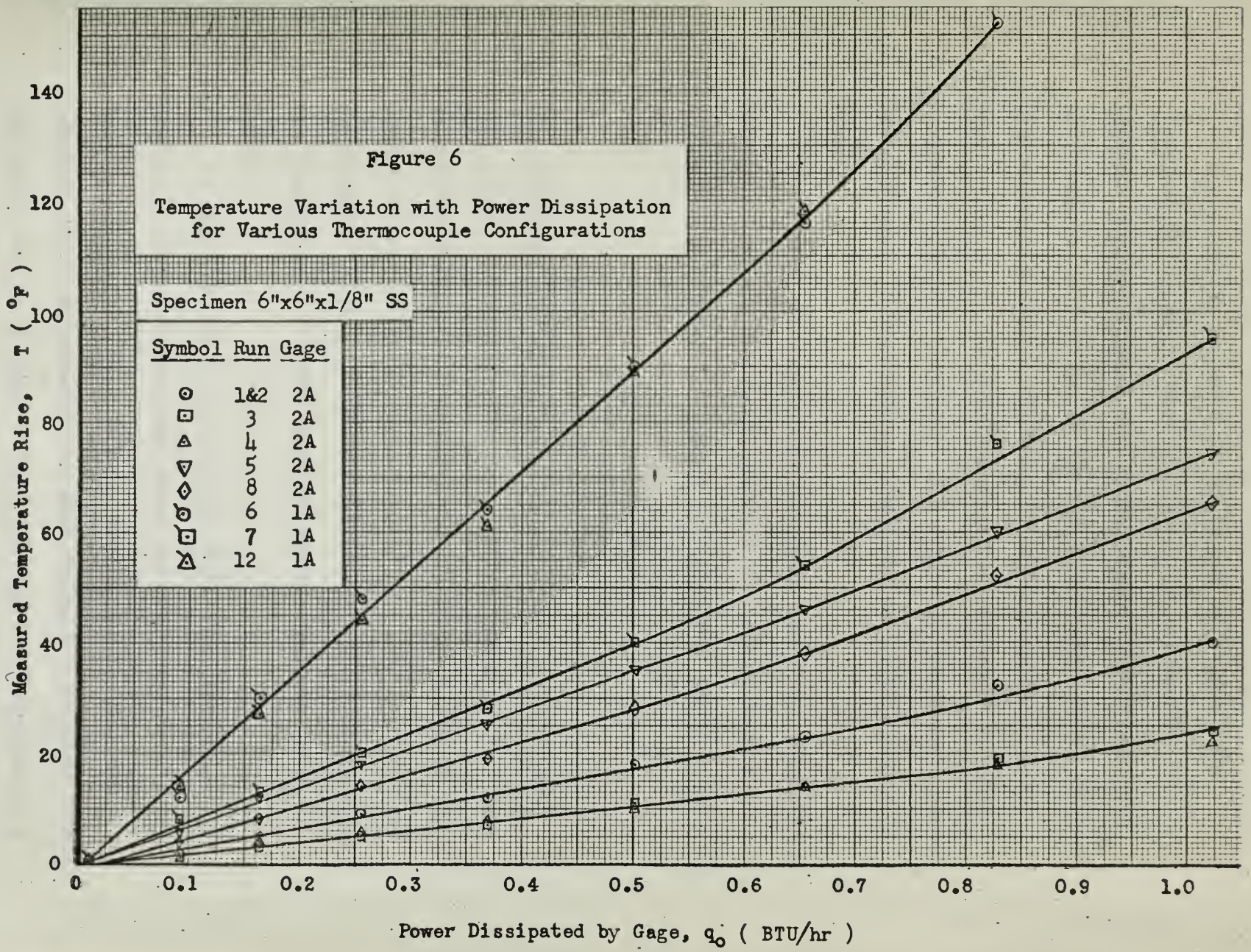
Figure 6
Temperature Variation with Power Dissipation for Various Thermocouple Configurations
Specimen 6"x6"x1/8" SS
Symbol Run Gage
1&2 2A
3 2A
4 2A
5 2A
8 2A
6 1A
7 1A
12 1A
Measured Temperature Rise, T (°F)
0
20
40
60
80
100
120
140
0
0.1
0.2
0.3
0.4
0.5
0.6
0.7
0.8
0.9
1.0
Power Dissipated by Gage, q_o (BTU/hr)

thermal resistance from Table II-8. It is immediately evident upon comparing the two sets of values that correlation is conspicuously lacking. From the discussion of Appendix III it is apparent that the thermal contact resistance between gage grid and thermocouple junction is the most significant reason for the discrepancies observed. No means of determining reasonable corrections for the measured temperatures to account for this resistance could be obtained. As a result the temperature measuring approach to system thermal resistance verification was abandoned.

The electrical resistance measurement method for determining the system thermal resistance provided the results from which the curves of Figures 7, 8, and 9 were plotted. Based on Eq. (18),

$$R_{th} = \frac{\Delta R_g / R_g}{I_g^2 R_g} \Big/ \eta \quad ,$$

the theoretical and experimental values of the system thermal resistance were determined as described in Appendix III. These values are listed in Tables III-2 and III-3 (pp. III-7, 8, and 9). General discussion concerning comparisons of the analytical and experimental values of these resistances will be found following the discussion of the more specific results demonstrated by the curves.

In Figure 7 the curves show the fractional electrical resistance change of the gage versus the gage power level for Runs 7, 8, and 12. These markedly demonstrate the non-linear behavior of the system when high gage currents (high power levels) are used. It may be observed that non-linearity commences at a

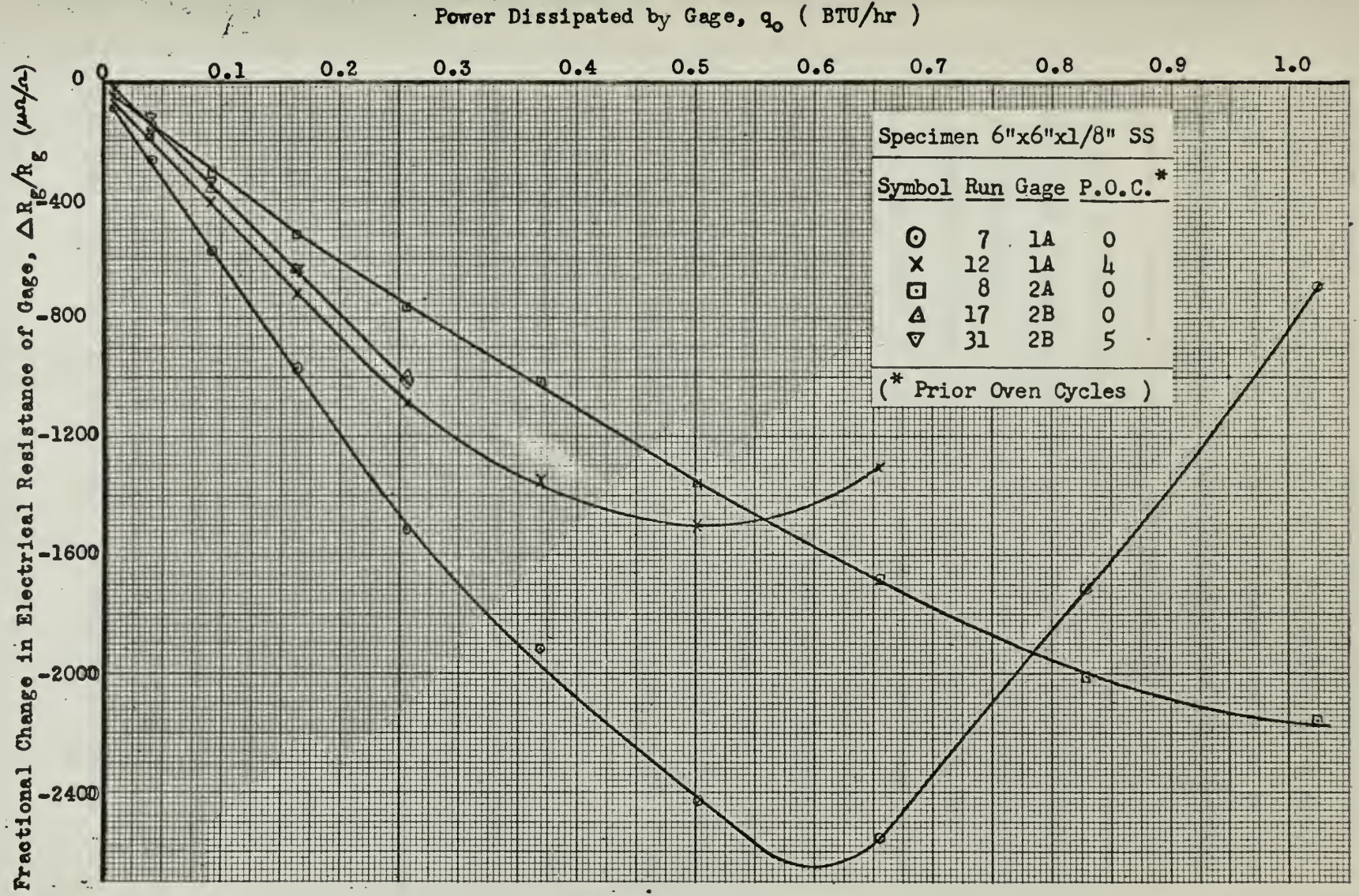

Figure 7

Effects of High Gage Currents, Thermal Cycling, and Gage Installation on Fractional Resistance Change

much lower power level for the smaller gage (1A in Runs 7 and 12) than for the larger (2A in Run 8). The curves for Runs 8 and 17 show the difference in gage performance which may be obtained between gages of the same type attached by the same technique to plates of identical material. The most significant effects to which this difference may be attributed are the thickness of the adhesive layer bonding the gage to the specimen and the degree of cure of the adhesive. This inconsistency is further demonstrated by comparing the curves for Run 7 with Run 12 and Run 17 with Run 31. Both pairs of curves include test runs performed before and after several thermal cycles in an oven. The first pair shows a marked difference between the resistance indications observed while the second shows almost no change at all. These curves of Figure 7 are included primarily as graphical examples of the problems encountered in trying to accurately predict strain gage performance.

The expression for the equivalent thermal resistance of the system developed in Appendices I and II is based on the approximations that neither the leads nor the exposed surfaces of the gage grid and tabs provide paths for appreciable heat dissipation compared with the path through the gage backing, adhesive and specimen. The tests designed to demonstrate the validity of these approximations are described in detail in Appendix III (p. III-4). Figure 8 shows the results of these tests. Runs 12 and 13 were made under the same conditions except that different size leads were used in each case. The maximum difference

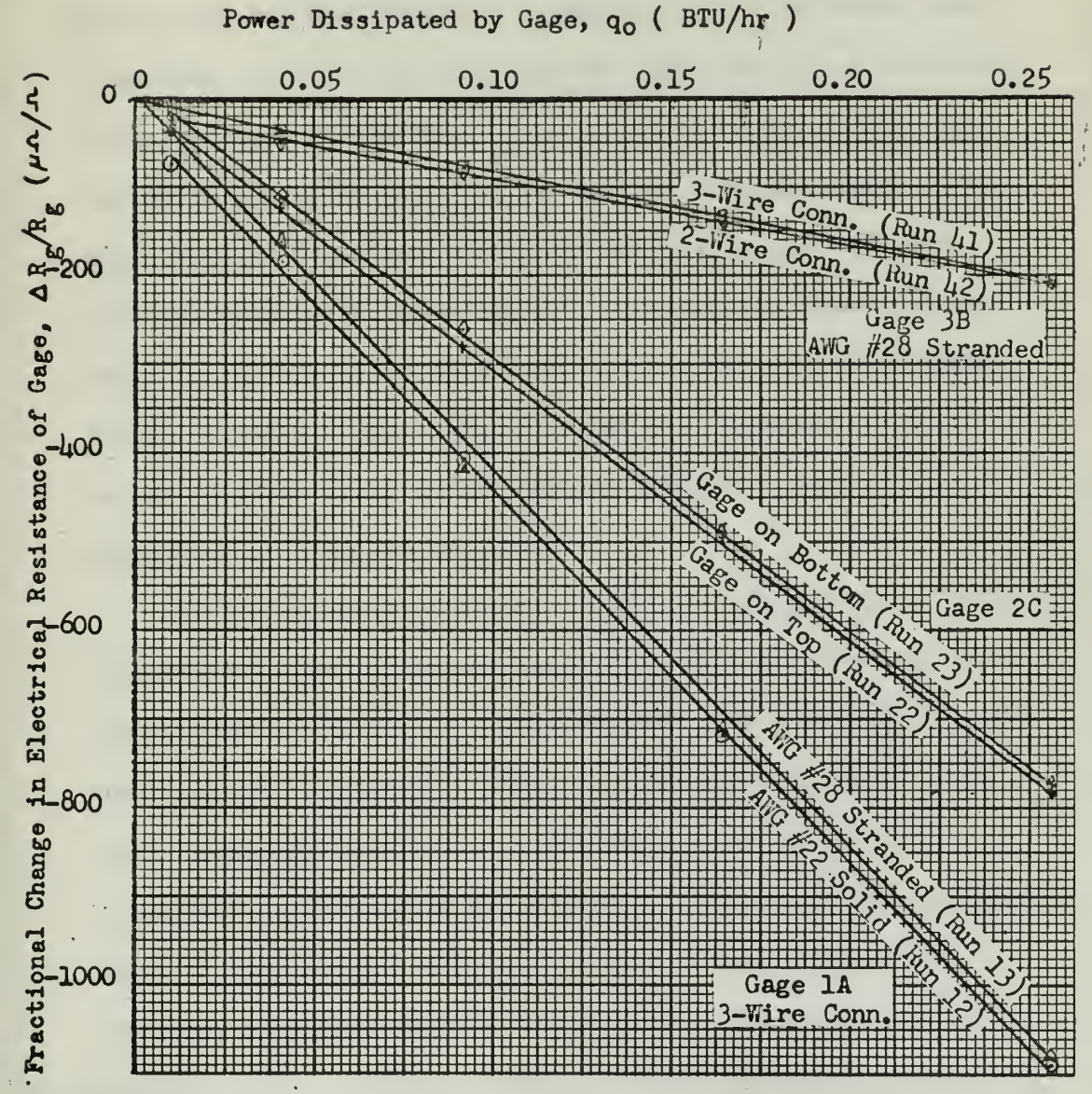

Figure 8

Effects of Lead Wires and Exposed Gage Surfaces on Heat Dissipation

between the two curves is about 20 $\frac{\mu\Omega}{\Omega}$. For a gage factor of 2 this amounts to an apparent strain of 10 $\frac{\mu \text{ in}}{\text{in}}$ which is negligible in most strain gage applications. Another set of tests showing the lead wire effects on the heat transfer mechanism is given by the curves for Runs 41 and 42. Except for the different gage connection circuitry as noted on the figure both runs were made under the same conditions. The difference between these two curves is less than that for the curves described above. From these results it is concluded that neglecting the lead wire effects was a valid approximation. The plotted results from Runs 22 and 23 for the gage facing upward and downward respectively indicate a negligible difference in apparent strain due to heat dissipation from the exposed surfaces. Hence, this approximation also appears valid.

The curves shown in Figure 9 (p. 40) indicate the effects of some of the other variables involved in the determination of the system thermal resistance. Runs 35, 38, and 39 demonstrate the minor effect of specimen surface area on the electrical resistance change and hence on the thermal resistance of the system. Comparing Runs 19 and 38 shows that the effect of plate thickness might be appreciable. Similarly, Runs 25 and 33 show that the effect of specimen material on the thermal resistance might also be appreciable. However, hidden in these latter two comparisons are the effects of adhesive and gage backing thickness and their conductivities which may vary from one installation to another. It can be shown from the calculations of Appendix II that the

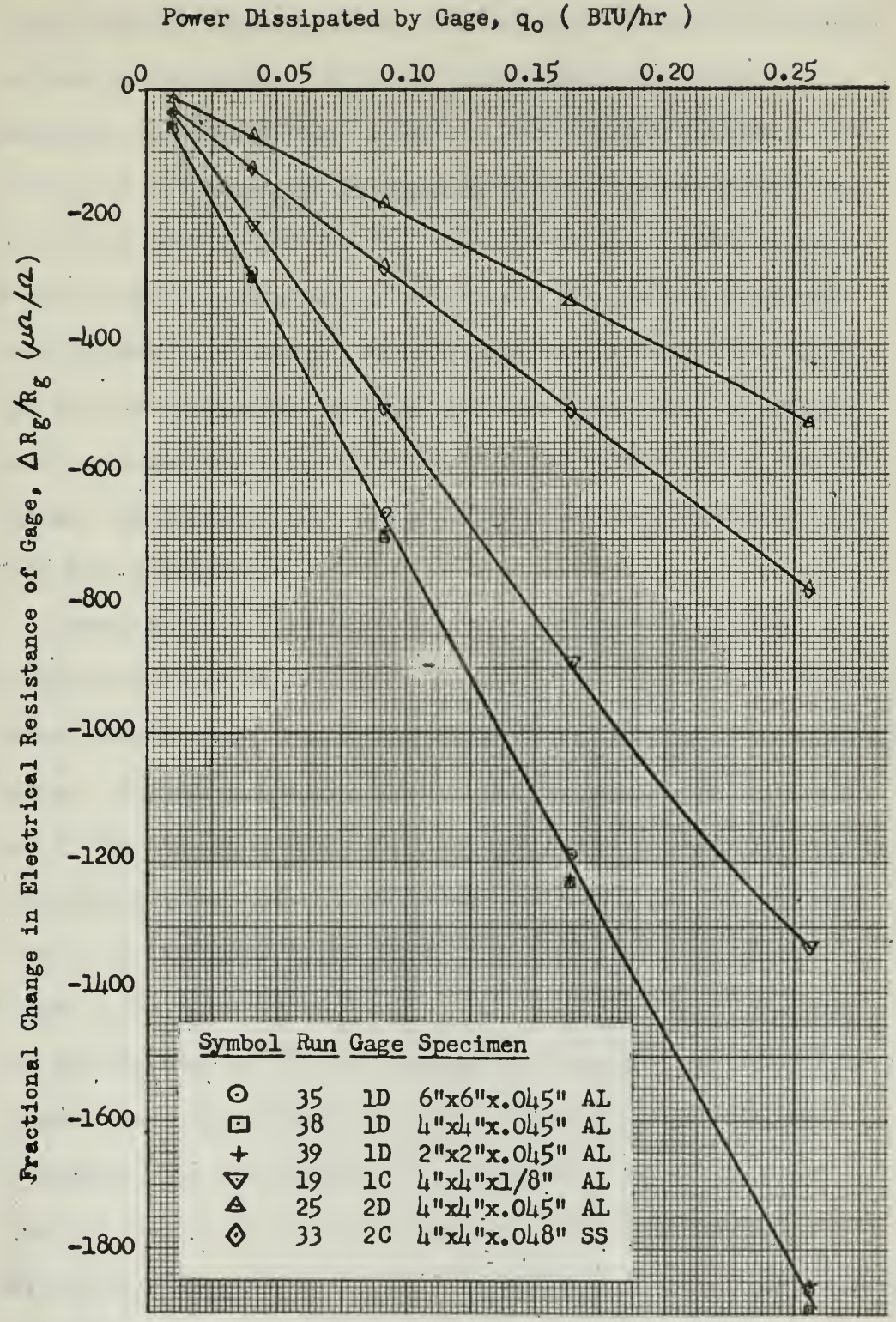

Figure 9

Effects of Specimen Thickness, Surface Area and Material, and Gage Size on Heat Dissipation

thermal resistance of the system might vary by about 40% due to these effects. Unfortunately, the same gage installation cannot be made on specimens of different thicknesses or different materials to isolate these effects. Overriding all these effects is that of the grid size as shown by the difference between the curves for Runs 25 and 38. It may also be noted from Figures 8 and 9 that the experimental slopes for the smaller gages are much steeper than that for the largest gage. Thus, even though the effects of specimen material and thickness might be appreciable in themselves, their fractional contribution to the overall thermal resistance of the system becomes less significant as the grid area decreases.

Examination of the calculated and experimental thermal resistances listed in Tables III-2 and III-3 shows that the experimental values range from about 10% above to 60% below the computed values. Excluding the results of tests performed with gages 1A and 1C the 60% value drops to about 30%. One explanation for the poor results from gage 1A, which provided the worst correlation, is that in the tests to demonstrate nonlinearity as shown in Figure 6 the maximum permissible gage temperature, specified by the manufacturer as 200°F, was probably exceeded. As previously stated, this would weaken the bond between gage and specimen. It appears that the weakening was permanent for this case and that the results of following tests with this gage might be questionable when compared with similar tests of other gages. The results with gage 1C can not be explained in this manner.

It is seen, then, that although the thermal resistance calculated from Eq. (13), or Eq. (14) for the smallest gages, does not correspond exactly with the experimental value, its use in Eq. (15) would provide a reasonable estimate for the grid temperature corresponding to a given gage current. As shown by the discussion above, these temperature values would be conservative in most cases.

5. Conclusions

Based on the analytical results of Section 2 and the experimental results of Appendix III as discussed in the previous section, conclusions regarding the temperature rise of the gage grid due to self-heating effects in very small resistance strain gages may be listed as follows:

(a) For the smallest gages the gage power dissipation per unit grid area is the dominant factor in predicting the steady-state grid temperature rise.

(b) For the smallest gages the thermal resistance of the system is almost completely attributable to that of the gage backing and the bonding adhesive, and is independent of the specimen size and material.

(c) In general the lead wires and the exposed surfaces of the gage grid and tabs provide paths for an insignificant fraction of the heat to be dissipated.

(d) In general the primary mechanism for self-heat dissipation from the gage is by conduction through the gage backing, bonding adhesive and specimen.

6. Bilbiography

1. Anonymous. Budd Metalfilm Strain Gages and Accessories. Catalog BG-2200, Instruments Division. The Budd Company, Phoenixville, Pa., Sept., 1961.

2. Anonymous. Eastman 910 Adhesive. Eastman Kodak Company, 1958.

3. Anonymous. Operating Instructions - Model BAM-1, Bridge Amplifier and Meter. Ellis Associates, Pelham, New York, 1959.

4. Anonymous. Precision Foil Strain Gages - Catalog No. 10, plus supplementary Specification and New Release Sheets. Micro-Measurements, Inc., Romulus, Michigan.

5. Anonymous. Strain Gage Handbook. Bulletin 4311 A - Electronics Division, Baldwin-Lima-Hamilton Corp., Waltham, Mass.

6. Anonymous. The Shippingport Pressurized Water Reactor. Addison Wesley Publishing Co., Reading, Mass., 1958.

7. Baker, H. D. Manual on Thermometry with Emphasis on Thermo-couple Techniques. United Aircraft Corp., East Hartford, Conn., 1950.

8. Baker, H. B., Ryder, M. E., and Baker, M. A. Temperature Measurement in Engineering, v. I, 1953; v. II, 1961: John Wiley and Sons, Inc.

9. Baumeister, T. (ed.) Mark's Mechanical Engineers Handbook, Sixth edition. McGraw-Hill Book Co., New York, 1958.

10. Bean, W. T. Strain Gage Accessories and Techniques. William T. Bean, Detroit, Michigan.

11. Bergman, S. and Schiffer, M. Kernel Functions and Elliptic Differential Equations in Mathematical Physics. Academic Press Inc., New York, 1953.

12. Bloss, R. L. Characteristics of Resistance Strain Gages. Semiconductor and Conventional Strain Gages (ed. Dean, M.) Academic Press, New York, 1962, pp. 123-142.

13. Bloss, R. L. Evaluation of Resistance Strain Gages at Elevated Temperatures. Materials Research and Standards, January, 1961. pp 9-15.

14. Campbell, J. B. (ed.). Materials Selector, 1959-1960 Ref. Issue. Materials in Design Engineering. v. 50, #5, Oct. 1959.

15. Campbell, W. R. Tests of Six Types of Bakelite-Bonded Wire Strain Gages. National Advisory Committee for Aeronautics Technical Note, No. 1656, July, 1948.

16. Carslaw, H. S. and Jaeger, J. C. Conduction of Heat in Solids. Oxford University Press, London, England, 1947.

17. Clark, W. Photography by Infrared. Second edition. John Wiley and Sons, Inc., New York, 1946.

18. Coover, H. W., et al. Chemistry and Performance of Cyanoacrylate Adhesives. Society of Plastics Engineers Journal, v. 15 #5, 1959.

19. Dusinberre, G. M. Heat Transfer Calculations by Finite Differences. International Textbook Co., Scranton, Pa., 1961.

20. Frados, J. (ed.). Modern Plastics Encyclopedia for 1964. Modern Plastics, v. 41 #1A, Sept.,1963.

21. Gardner, K. A. Efficiency of Extended Surfaces. American Society of Mechanical Engineers, Transactions, v. 67, 1945, pp 621-631.

22. Gray, A., Mathews, G. B., and MacRobert, T. M. A Treatise on Bessel Functions and Their Applications to Physics. Second edition. MacMillan and Co., Ltd. London, 1931.

23. Hackforth, H. L. Infrared Radiation. McGraw-Hill Book Co., Inc. New York, 1960.

24. Hannah, R. L. and Kinan, A. M. Measuring Strain to 1000° F. Instruments and Control Systems. v. 33, July, 1960, pp. 1166-1168.

25. Hathaway, C. M. Strain-Gage Instrumentation. Instruments and Automation. v. 31, March 1958, pp 450-454.

26. Hayes Aircraft Corporation. An Introduction to the Principles of Infrared Physics. Third edition. Commercial Printing Co., Birmingham, Ala., 1958.

27. Herczeg, L. and Beckman, P. High Temperature Strain Gages. Instruments and Automation. v. 31, March, 1958, pp 460-461.

28. Higson, G. R. Resistance Strain Gauges of Low Temperature Sensitivity. Journal of Scientific Instruments. v. 36, April, 1959, pp 157-159.

29. Hines, F. F. and Weymouth, L. J. Practical Aspects of Temperature Effects on Resistance Strain Gages. Semiconductor and Conventional Strain Gages (ed. Dean, M.) Academic Press, New York, 1962, pp. 143-168.

30. Hodgman, G. D. (ed.). Handbook of Physics and Chemistry, 37th edition, Chemical Rubber Co., Cleveland, Ohio, 1955.

31. Jakob, M. Heat Transfer. v. I, John Wiley and Sons, Inc., New York, 1949.

32. Jones, E. and Maslen, K. R. The Physical Characteristics of Wire Resistance Strain Gages. Aeronautical Research Council Reports and Memoranda #2661, Nov. 1948. Her Majesty's Stationery Office, London, 1952.

33. Kreith, F. Principles of Heat Transfer. International Textbook Co., Scranton, Pa., 1958.

34. Le Gette, M. A. Strain-Gage Principles. Instruments and Automation. March 1958, pp. 447-449.

35. Littlejohn, H. F. Jr. Handbook of Power Resistors, Second edition. Ward Leonard Electric Co., Mount Vernon, New York, 1956.

36. Lyman, T. (ed.). Metals Handbook. v. I, Eighth edition, American Society for Metals, Novelty, Ohio, 1961.

37. Modlin, D. L. Method for Computing Temperature Characteristic of a Wire-Wound Strain Gage. Measurement Techniques--Soviet Instrumentation and Control Translation Series, June, 1963.

38. Mueller, G. V. Introduction to Electrical Engineering, Second edition. McGraw-Hill Book Co., New York, 1948.

39. Murray, W. M. Strain Gage Types and Basic Circuits. Instrument Society of America Journal, v. 9, #2, Feb. 1962, pp 47-51.

40. Murray, W. M. What Are Strain Gages - What Can They Do? Instrument Society of America Journal, v. 9, #1, Jan., 1962, pp 30-36.

41. Ovrebo, P. J. et al. Industrial, Technical and Medical Applications of Infrared Techniques. Procedings of the Institute of Radio Engineers. v. 47, #9, Sept., 1959, pp 1629-1645.

42. Perry, C. C. and Lissner, H. R. The Strain Gage Primer, Second edition. McGraw-Hill Book Co., Inc., New York, 1962.

43. Preckshot, G. W. and Gorman, J. W. Steady-State Longitudinal and Radial Temperature Distributions in Internally Heated Finite Wires. Industrial and Engineering Chemistry. v. 50, #5, May, 1958, pp 837-848.

44. Schneider, P. J. Conduction Heat Transfer. Addison-Wesley Publishing Co., Inc. Cambridge, Mass., 1955.

45. Scott, I. G. Some Temperature Effects on Resistance Strain Gages. Semiconductor and Conventional Strain Gages (ed. Dean, M.). Academic Press, New York, 1962, pp 73-91.

46. Sommerfield, A. Partial Differential Equations in Physics. Academic Press Inc., New York, 1949.

47. Stein, P. K. Adhesives: How They Determine and Limit Strain Gage Performance. Semiconductor and Conventional Strain Gages (ed. Dean, M.) Academic Press, New York, 1962.

48. Stein, P. K. Measurement Engineering. v. I and II. Second edition. Stein Engineering Services, Inc., 1962.

49. Watson, G. J. A Treatise on the Theory of Bessel Functions. Second edition. The Macmillan Co., New York, 1945.

APPENDIX I

DEVELOPMENT OF THERMAL RESISTANCE PARAMETERS

1. Resistance to Heat Flow from Gage Grid to Tab (R_t)

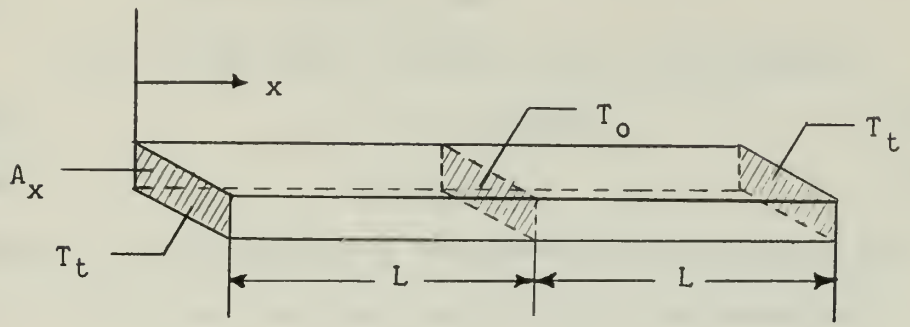

Figure I-1
Sketch illustrating nomenclature for heat conduction in a single conductor with internal heat generation.

For a single electrical conductor of rectangular geometry, as shown in Figure I-1, and insulated from its surroundings in the y and z directions it can be shown /33-41/ that the temperature variation with length due to an electrical current passing through it in the x direction is:

$$T - T_t = (\dot{q}L^2/2k)\left[2(x/L) - (x/L)^2\right] \qquad (I\text{-}1)$$

where: T is the local temperature,

$\dot{q}$ is the heat generated (to be dissipated) per unit volume and time,

L is half the length of the conductor,

k is the thermal conductivity of the conductor, and

x is the position relative to the end of the conductor.

Taking the derivative of $(T-T_t)$ with respect to x and equating to zero yields the maximum temperature location at the mid-length

of the conductor (at $x = L$). Letting $T_o = T_{max}$, then

$$T_o - T_t = \dot{q}L^2/2k . \qquad (I-2)$$

But

$$\dot{q} = q_t/LA_x \qquad (I-3)$$

where: q_t is the heat flow rate from mid-span to the end of the conductor, and

A_x is the cross sectional area of the conductor.

Then

$$T_o - T_t = q_t L/2kA_x . \qquad (I-4)$$

Also

$$R = 2\rho L/A_x \qquad (I-5)$$

where: R is the electrical resistance of the conductor and

ρ is the electrical resistivity of the conductor material.

Eliminating A_x from Eqs. (I-4) and (I-5) yields

$$T_o - T_t = q_t R / 4\rho k \qquad (I-6)$$

Considering the gage grid to be of uniform cross section and stretched out forming a straight conductor of this type it is asserted that, as a first approximation, the thermal resistance between the point of maximum grid temperature and that at a gage tab is, from Eq. (I-6),

$$R_t' = (T_o - T_t)/ q_t = R_g / 4\rho_g k_g \qquad (I-7)$$

where T_o is the maximum grid termperature

T_t, q_t, and R_g as defined in Section 1,

ρ_g is the electrical resistivity of the gage material, and

k_g is the thermal conductivity of the gage material.

Note that R_t', as determined by Eq. (I-7), is based on the difference between the maximum grid temperature and the average tab temperature. The value of R_t to be used in the circuit of Figure 2, however, is based on the difference between the

average grid and tab temperatures. It is necessary, therefore, to define a coefficient, C, such that

$$(\overline{T}_o - T_t) \,/\, q_t = R_t = C\, R_t' \qquad \text{(I-8)}$$

where C is based on the relationship between the maximum and average temperatures of the gage grid.

Again considering the grid as a straight conductor, a combination of Eqs. (I-1) and (I-2) yields

$$T - T_t = (T_o - T_t)\left[2(x/L) - (x/L)^2\right] \qquad \text{(I-9)}$$

The average value of this distribution may be determined from

$$\frac{\displaystyle\int_0^2 \frac{T - T_t}{T_o - T_t}\, d\left(\frac{x}{L}\right)}{\displaystyle\int_0^2 d\left(\frac{x}{L}\right)} = \frac{2}{3} \qquad \text{(I-10)}$$

This value may be recognized as the ratio of the average to maximum value for a parabolic distribution. Hence, for the straight conductor

$$\overline{T}_o - T_t = \frac{2}{3}(T_o - T_t) \quad . \qquad \text{(I-11)}$$

Further, it is asserted here, and shown by the calculations of Appendix II, that $T_t \approx T_\infty$ whence

$$\overline{T}_o - T_\infty \approx \frac{2}{3}(T_o - T_\infty)\,. \qquad \text{(I-12)}$$

Combining Eqs. (I-7), (I-8), and (I-12) shows that

$$C = \frac{2}{3} \qquad \text{or} \qquad R_t = \frac{2}{3} R_t' \qquad \text{(I-13)}$$

Then, from (I-7) and (I-13), the thermal resistance based on the average grid temperature is

$$R_t = R_g \,/\, 6 \rho_g k_g \,. \qquad \text{(I-14)}$$

In actuality, the periphery of the conductor is not insulated and heat is dissipated through these surfaces. However, this additional heat dissipation is accounted for in the surface and specimen paths of the circuit. Hence, the assumption of an insulated conductor for this particular heat path appears valid.

The major discrepancy introduced by use of this straight conductor approximation is that in the actual case, with the grid in its "folded" configuration, there would be thermal interaction between the filaments of the grid involving all three modes of heat transfer. However, because of the minute geometry of the grid and the small temperature differences between adjacent filaments it is expected that these effects are minor. Therefore, it appears safe to assume that the average temperature of the gage grid is closely approximated by that of the straight conductor.

Further, for the particular case of determining R_t, it will be seen, from the calculations in Appendix II, that the magnitude of R_t from Eq. (I-14), relative to the other parameters of the system, is such that this discrepancy is inconsequential.

2. Resistance to Heat Flow Through a Lead Wire (R_ℓ)

Considering the lead wire as an infinitely long, rod-type fin with a source temperature equal to the average tab temperature (T_t) it can be shown /33-47/ that the heat removed from the tab by the lead, per unit time, is

$$q_\ell = \sqrt{h' P k_c A_c}\ (T_t - T_\infty) \qquad \text{(I-15)}$$

where: h' is a combined heat transfer coefficient including conduction through lead insulation and convection from the surface,

$P = 2\pi r_i$ is the perimeter of the outside surface of the insulation,

k_c is the thermal conductivity of the conductor material,

$A_c = \pi r_c^2$ is the cross sectional area of the conductor,

r_c is the outer radius of the insulation.

Then,

$$R_\ell = \frac{T_t - T_\infty}{q_\ell} = \frac{1}{\sqrt{h' P k_c A_c}} = \frac{1}{\pi r_c \sqrt{2h' k_c r_i}} \,. \qquad \text{(I-16)}$$

And, from basic linear heat flow theory /33-35/,

$$h' = \frac{1}{\frac{1}{h} + \frac{r_i \ln (r_i/r_c)}{k_i}} \qquad \text{(I-17)}$$

where h is the mean heat transfer coefficient for the outer insulation surface,*

k_i is the thermal conductivity of the insulating material.

*Convection, as used throughout, is composed of natural convection, radiation and surface resistance (scale, etc.) such that the local heat flux across the surface is $h(T-T_\infty)$. In actuality, then, h is a combined heat transfer coefficient for the surface.

Since the leads are not of infinite length a correction can be made /33-49/ such that

$$q_{\ell} \text{ (finite)} = q_{\ell} \text{ (infinite)} \tanh m\ell \qquad \text{(I-18)}$$

where:

$$m = \sqrt{\frac{h'P}{k_c A_c}} \quad (ft^{-1})$$

ℓ is the length of lead in feet.

It will be seen from the calculations of Appendix II(p.II-4) that, for typical leads, m has a magnitude such that $\tanh m\ell = 1$ for leads of approximately one foot or more in length. Hence, the assumption of infinitely long leads is valid for this case.

It is to be noted that this development does not include any local effects at the soldered junction between lead and tab (or lead to terminal strip to pigtail to gage tab in those installations where terminal strips are used). This was originally omitted for the sake of simplicity and not added later since the entire lead resistance term is shown to have little effect on the overall system. (See Appendices II and III.)

3. Resistance to Heat Flow at Exposed Surface

(a) From Gage Tab (R_s)

From basic heat transfer theory /33-14/ assuming that the tab is at uniform temperature and that the area of the heat transfer surface is that of the tab, the rate of heat transfer by convection between the surface and adjacent air is

$$q_s = h A_t (T_t - T_\infty) \qquad \text{(I-19)}$$

where h, T_t, and T_∞ are as previously defined and A_t is the surface area of the gage tab.

Then

$$R_s = \frac{T_t - T_\infty}{q_s} = \frac{1}{h A_t} \quad . \qquad \text{(I-20)}$$

It has been found from measurements on several gages that a fair approximation for the area of one tab is

$$A_t' = \frac{1}{3} (A_o - A_g) \qquad \text{(I-21)}$$

where: A_o is the overall area of the gage including tabs, and

A_g is the area of the gage grid excluding loop ends of the grid filaments.

The assumptions made in obtaining this parameter, R_s, appear to be justified for the same reasons as stated in the last paragraph of Section I-2 for the lead resistance.

If there is a layer of material covering the tabs (e.g., paper, epoxy, waterproofing compound) a resistance parameter similar to those developed in Sections I-4 and

I-5 (below) involving tab area, covering thickness and thermal conductivity of the covering material must be added in series with R_s. This resistance would appear at the left of R_s in Figure 2.

(b) From Gage Grid (R_a)

Considering the gage grid as a plane surface of area A_g equal to the product of gage length by grid width (as defined in Appendix II) and at a uniform temperature $\bar{T}_o$ this parameter may be obtained in exactly the same manner as that for the tab. Hence,

$$R_a = \frac{\bar{T}_o - T_\infty}{q_a} = \frac{1}{h A_g} \qquad \text{(I-22)}$$

If a gage covering exists additional resistance must be included in series as above.

The assumption of a plane heat transfer surface of area A_g may be justified by taking into account the fact that the actual heat transfer surface includes the sides of the grid filaments as well as the top and sides of the loop ends. This additional area could be considered to fill in the spaces between the upper faces of the grid filaments, thus completing the area such that A_g equals gage length times grid width.

The uniform temperature, $\bar{T}_o$, shown in equation (I-22) is the average temperature developed in Section I-1 and shown on the schematic diagram of Figure 2.

4. Resistance to Heat Flow through Gage Backing Material

(a) Under Gage Tab (R_{bt})

Utilizing the assumptions of Section I-3(a) and considering linear heat flow, the rate of heat conducted through the backing, from basic theory /16-2; 33-11; 44-2/ is

$$q_b = \frac{k_b A_t (T_t - T_{mt})}{d_b} \qquad (I-23)$$

where A_t, T_t, and T_{mt} are as previously defined, k_b is the thermal conductivity of the backing material and d_b is the thickness of the backing material.

Hence,

$$R_{bt} = \frac{T_t - T_{mt}}{q_b} = \frac{d_b}{k_b A_t} \qquad (I-24)$$

(b) Under Gage Grid (R_{bg})

Based on the assumptions of Section I-3(b) the backing resistance under the grid is obtained by the procedure given above for the tab. Thus,

$$R_{bg} = \frac{\overline{T}_o - T_{mg}}{q_p} = \frac{d_b}{k_b A_g} \qquad (I-25)$$

5. Resistance to Heat Flow Through Bonding Adhesive

(a) Under Gage Tab (R_{ct})

Following the same argument as in Section I-4(a)

$$R_{ct} = \frac{T_{mt} - T_{pt}}{q_b} = \frac{d_a}{k_a A_t} \qquad \text{(I-26)}$$

where A_t, T_{mt}, and T_{pt} are as previously defined, d_a is the thickness of the adhesive and k_a is the thermal conductivity of the adhesive.

(b) Under Gage Grid (R_{cg})

In the same manner

$$R_{cg} = \frac{T_{mg} - T_{pg}}{q_p} = \frac{d_a}{k_a A_g} \qquad \text{(I-27)}$$

with all parameters as previously defined.

6. Resistance to Heat Flow Through The Specimen and Its Surfaces

(a) Under Gage Grid (R_{pg})

An exact analytical solution of the heat transfer problem involving a very small (geometrically) heat source on the surface of a metallic specimen would, at best, be most complex. Such a solution may be obtained by various means from material presented in the literature. /11; 16; 19; 21; 22; 31; 33; 44; 46; 49/. However, the object of developing these thermal resistance parameters was to establish a relatively simple relationship between gage temperature and gage current which may be used without excessive calculations. In addition, it will be seen from the calculations of Appendix II that the magnitude of the thermal resistance obtained from the following derivation, relative to the other significant parameters of the system, is such that a good deal of latitude can be tolerated without serious overall effect. Hence, the procedure used is considered adequate for the purpose.

Several tests were made using an electric soldering iron as a heat source at the center of the upper surface of a horizontal, square, flat plate, analogous to the gage installation. The iron was insulated so that only the tip, which had about the same contact area as a gage, was exposed. This method provided a much greater heat flux than the gage and resulted in

higher temperatures throughout the plate which made the temperature variation on the surface more discernible. It was found that the temperature distribution on both the upper and lower surfaces exhibited very little angular dependence and that, beginning at a short distance from the center, the top and bottom temperatures at a given radius were approximately equal. Based on these findings, the heat transfer model illustrated in Figure I-2 was devised to represent the gage installation.

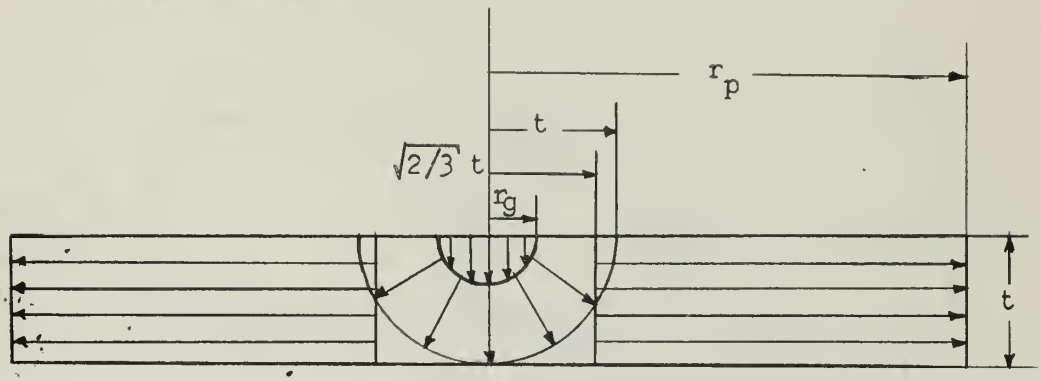

Figure I-2
Analytical model for approximate heat transfer analysis of a flat plate with a small surface source.

In Figure I-2 the heat conducted from the gage grid is considered to flow vertically downward through a small hemisphere of radius r_g, the equivalent radius of the gage; then radially from the small hemispherical surface to one of larger radius, t, equal to the plate thickness. At this point a transition is made from the spherical to cylindrical geometry. The

hemisphere of radius t is replaced by a cylinder having the same volume and depth. The temperature of the bottom and lateral surfaces of the equivalent cylinder is assumed to equal that of the curved surface of the original hemisphere. Then, in cylindrical coordinates, the heat flows radially from the periphery of this inner cylinder as in a circumferential fin. The heat paths described above are modified near the surfaces because of convection from the exposed faces.

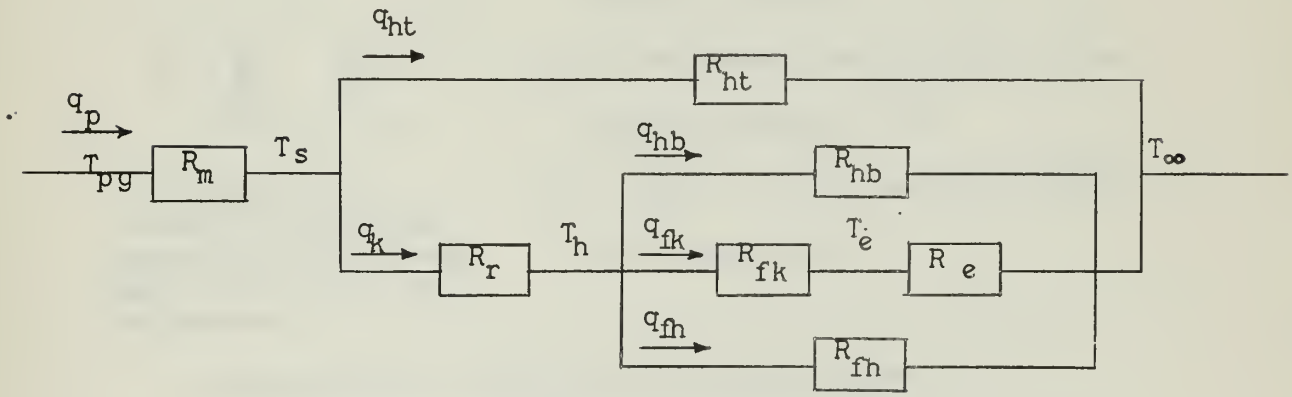

Figure I-3
Schematic Diagram of Steady State Heat Transfer Mechanism Through Specimen

Figure I-3 is a schematic diagram of the heat transfer "circuit" for this sub-system. The nomenclature of the figure is defined below in conjunction with the derivations of the individual thermal resistance parameters of the sub-system.

The first component of the sub-system to be investigated is the small hemisphere directly under the

gage grid with a radius equal to the equivalent grid radius, r_g. Considering heat flow to be in the z direction only (See Figure I-4) from the isothermal plane at temperature T_{pg}* on top to the isothermal hemispherical surface at temperature T_s at radius r_g, the general conduction equation in incremental form becomes

$$dq_p = \frac{k_p(2\pi r\, dr)(T_{pg} - T_s)}{\sqrt{r_g^2 - r^2}} \qquad \text{(I-28)}$$

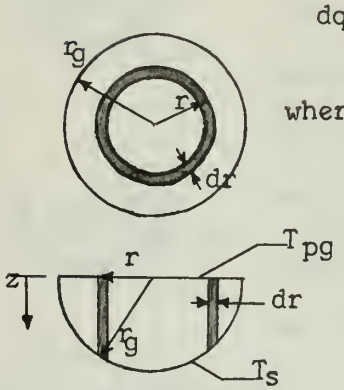

Figure I-4
Sketch illustrating nomenclature for linear heat flow through small hemisphere.

where: q_p and T_{pg} are as previously defined,

T_s is the temperature of the hemispherical surface,

k_p is the thermal conductivity of the specimen material, and

$r_g = \sqrt{A_g/\pi}$ is the equivalent radius of the gage grid.

Integrating both sides over the surface yields

$$q_p = (T_{pg} - T_s)\, 2\pi k_p r_g \,. \qquad \text{(I-29)}$$

The assumption of an isothermal curved surface leads to a temperature discontinuity at the intersection of the upper plane with the surface. However, because of the manner in which these temperatures are

*T_{pg} is the average temperature of the plate surface under the gage. The actual temperature is higher at the center than at the edges thus requiring a longer conduction path to be decreased to T_s.

used in the following steps and in view of the other approximations employed, this discontinuity can be accepted as having little effect on the overall parameter. The thermal resistance of this part of the model is then defined, from (I-29), as

$$R_m = \frac{T_{pg} - T_s}{q_p} = \frac{1}{2\pi k_p r_g} \quad . \qquad \text{(I-30)}$$

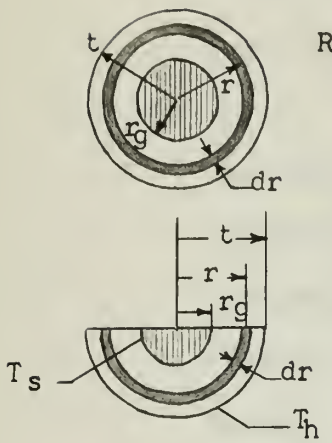

Figure I-5
Sketch illustrating nomenclature for heat flow through concentric hemispherical shells.

Next, the form for the thermal resistance of the material between r_g and t is obtained by considering that all of the heat flows radially through concentric hemispherical shells of incremental thickness (Figure I-5) For this case the conduction equation becomes

$$q_p = -k_p(2\pi r^2)\frac{dT}{dr} \quad . \qquad \text{(I-31)}$$

Separating variables and setting up the integrals

$$\int_{r_g}^{t} \frac{dr}{r^2} = -\frac{2\pi k_p}{q_p} \int_{T_s}^{T_h} dT \qquad \text{(I-32)}$$

where: t is the thickness of the specimen,

T_h is the temperature of the hemispherical surface at radius t, and all other parameters are as previously defined.

from which

$$\frac{t - r_g}{t r_g} = \frac{2\pi k_p}{q_p}(T_s - T_h) \quad . \qquad \text{(I-33)}$$

Defining the resistance of this section as

$$R_r = \frac{T_s - T_h}{q_p} = \frac{t - r_g}{2\pi k_p t r_g} = R_m \frac{t - r_g}{t} \qquad \text{(I-34)}$$

then the total conductive resistance to this point is

$$R_m + R_r = \frac{T_{pg} - T_h}{q_p} = R_m \frac{2t - r_g}{t} = \frac{2t - r_g}{2\pi k_p t r_g} \quad . \qquad \text{(I-35)}$$

Note, from Eq. (I-35), if $2t \gg r_g$

$$R_m + R_r \approx 2R_m \qquad \text{(I-36)}$$

for conduction alone. Also note that because of the convection from the upper surface of this hollow hemisphere all of the heat does not flow all the way through the shell. Denoting the heat which does flow through the shell as q_k, the resistance of Eq. (I-34), compatible with Figure I-3, is

$$R_r = \frac{T_s - T_h}{q_k} = \frac{t - r_g}{2\pi k_p t r_g} = R_m \frac{t - r_g}{t} \quad . \qquad \text{(I-37)}$$

As previously described (p. I-12), the transition from spherical to cylindrical geometry is now made by replacing the hemisphere discussed above with an equivalent cylinder of the same volume and depth. For this inner cylinder

$$\text{Volume} = \frac{2}{3}\pi t^3 = \pi r^2 t \qquad \text{(I-38)}$$

from which the radius of the equivalent cylinder is $\sqrt{2/3}\ t$.

Next, considering radial heat flow in the outer hollow cylinder the conduction equation takes the form

$$q_{fk} = -k_p (2\pi r t) \frac{dT}{dr} \quad . \qquad \text{(I-39)}$$

Separating variables and setting up the integrals

$$\int_{T_h}^{T_e} \frac{dT}{q_{fk}} = -\frac{1}{2\pi k_p t} \int_{\sqrt{2/3}\,t}^{r_p} \frac{dr}{r} \qquad \text{(I-40)}$$

from which the conductive thermal resistance is

$$R_{fk} = \frac{T_h - T_e}{q_{fk}} = \frac{1}{2\pi k_p t} \ln \frac{r_p}{\sqrt{2/3}\,t} \qquad \text{(I-41)}$$

where: $r_p = \sqrt{A_p/\pi}$ is the equivalent radius of the plate,

A_p = the area of the surface on which the gage is attached, and

T_e is the temperature of the surface at the outer periphery of the plate.

The heat dissipated per unit time to the atmosphere from the outer edge of the specimen is given by

$$q_{fk} = h(2\pi r_p t)(T_e - T_\infty). \qquad \text{(I-42)}$$

The thermal resistance at this surface is then

$$R_e = \frac{T_e - T_\infty}{q_{fk}} = \frac{1}{2\pi h r_p t} \,. \qquad \text{(I-43)}$$

The total resistance of the q_{fk} leg of the circuit in Figure I-3 then becomes, from Eqs. (I-41) and (I-43),

$$R_{fk} + R_e = \frac{\ln \frac{r_p}{\sqrt{2/3}\,t}}{2\pi k_p t} + \frac{1}{2\pi h r_p t} = \frac{T_h - T_\infty}{q_{fk}} \qquad \text{(I-44)}$$

whence

$$q_{fk} = (T_h - T_\infty) \frac{2\pi h k_p t r_p}{k_p + h r_p \ln \frac{r_p}{\sqrt{2/3}\,t}} \,. \qquad \text{(I-45)}$$

The heat dissipated from the upper and lower surfaces of the fin portion of the specimen is obtained next. Assuming that both faces have the same temperature distribution and the same surface coefficient of heat transfer, the convection equation, in incremental form, is

$$dq_{fh} = 2h(2\pi r\, dr)(T-T_\infty). \qquad (I-46)$$

Since both surfaces are being considered in (I-46) the right side has been multiplied by two. The temperature distribution for this region is obtained in the same manner as T_e in (I-41) such that

$$T = T_h - q_{fk} \frac{\ln \frac{r}{\sqrt{2/3}\, t}}{2\pi k_p t}. \qquad (I-47)$$

Using this function in (I-46)

$$q_{fh} = 4\pi h \int_{\sqrt{2/3}\, t}^{r_p} \left[T_h - T_\infty - q_{fk} \frac{\ln \frac{r}{\sqrt{2/3}\, t}}{2\pi k_p t} \right] r\, dr. \qquad (I-48)$$

Carrying out the integration yields

$$q_{fh} = 2\pi h(T_h - T_\infty)\left(r_p^2 - \frac{2}{3} t^2\right)$$

$$-q_{fk} \frac{h}{k_p t} \left[r_p^2 \ln \frac{r_p}{\sqrt{2/3}\, t} - \frac{1}{2} \left(r_p^2 - \frac{2}{3} t^2\right) \right]. \qquad (I-49)$$

Then, inserting q_{fk} from (I-45) the heat dissipated from these faces becomes

$$q_{fh} = 2\pi h (T_h - T_\infty) \left\{ \left(r_p^2 - \frac{2}{3}t^2\right) - \left[\frac{r_p^2 \ln \frac{r_p}{\sqrt{2/3}\,t} - \frac{1}{2}\left(r_p^2 - \frac{2}{3}t^2\right)}{\ln \frac{r_p}{\sqrt{2/3}\,t} + \frac{k_p}{h r_p}} \right] \right\} . \tag{I-50}$$

Hence, the combined thermal resistance of both the upper and lower surfaces is

$$R_{fh} = \frac{T_h - T_\infty}{q_{fh}} = \frac{1}{2\pi h \left\{ \left(r_p^2 - \frac{2}{3}t^2\right) - \left[\frac{r_p^2 \ln \frac{r_p}{\sqrt{2/3}\,t} - \frac{1}{2}\left(r_p^2 - \frac{2}{3}t^2\right)}{\ln \frac{r_p}{\sqrt{2/3}\,t} + \frac{k_p}{h r_p}} \right] \right\}} . \tag{I-51}$$

Yet to be obtained are the thermal resistances of the upper and lower surfaces of the central cylinder. Since it was previously assumed that the bottom face of the central cylinder is at temperature T_h, the heat flow rate from this surface is simply

$$q_{hb} = h\left(\frac{2}{3}\pi t^2\right)(T_h - T_\infty) \tag{I-52}$$

from which the corresponding thermal resistance is

$$R_{hb} = \frac{T_h - T_\infty}{q_{hb}} = \frac{3}{2\pi h t^2} . \tag{I-53}$$

On the upper surface heat is lost only from the area between r_g and $\sqrt{2/3}\,t$ since the heat source (gage grid) covers the area within the radius r_g. The heat dissipated from this area, obtained in the same manner as that from the fin surfaces, is

$$q_{ht} = \pi h (T_s - T_\infty)\left(\frac{2}{3}t^2 - r_g^2\right) - q_k \frac{h}{2K_p r_g}\left(\sqrt{\frac{2}{3}}t - r_g\right)^2 . \qquad \text{(I-54)}$$

From Figure I-3 it can be seen that q_k may be obtained by dividing the temperature drop $T_s - T_\infty$ by the combined resistance of R_r, R_{hb}, R_{fk}, R_e, and R_{fh}. The equivalent resistance for the combination of all these except R_r is

$$R_{comb} = \frac{1}{\frac{1}{R_{hb}} + \frac{1}{R_{fk} + R_e} + \frac{1}{R_{fh}}} . \qquad \text{(I-55)}$$

Taking R_{hb} from (I-53), R_{fk} from (I-41), R_e from (I-43) and R_{fh} from (I-51) this equivalent resistance becomes

$$R_{comb} = \frac{\ln \frac{r_p}{\sqrt{2/3}\,t} + \frac{k_p}{h r_p}}{2\pi h\left[\frac{k_p}{h}(r_p + t) + \frac{r_p^2}{2} - \frac{t^2}{3}\left(1 + \ln \frac{r_p}{\sqrt{2/3}\,t} + \frac{k_p}{h r_p}\right)\right]} . \qquad \text{(I-56)}$$

Then, using R_r from (I-37) and R_{comb} from (I-56)

$$q_k = \frac{T_s - T_\infty}{R_r + R_{comb}} \qquad \text{(I-57)}$$

and

$$q_{ht} = \pi h (T_s - T_\infty)\left\{\left(\frac{2}{3}t^2 - r_g^2\right) - \left(\sqrt{\frac{2}{3}}t - r_g\right)^2\left[\frac{1}{1 + (r_g/t)(2\pi k_p t R_{comb} - 1)}\right]\right\} \qquad \text{(I-58)}$$

from which

$$R_{ht} = \frac{1}{\pi h\left(\sqrt{\frac{2}{3}}t - r_g\right)\left(\sqrt{\frac{2}{3}}t + r_g\right) - \left(\sqrt{\frac{2}{3}}t - r_g\right)\left[\frac{1}{1 + (r_g/t)(2\pi k_p t R_{comb} - 1)}\right]\Bigg\}} . \qquad \text{(I-59)}$$

Having established the expressions for all of the individual thermal resistance parameters of Figure I-3, the resistance to heat flow through the specimen under the grid, R_{pg}, is their combined equivalent. As previously stated, the total resistance of the q_k leg is the sum $R_r + R_{comb}$. The calculations of Appendix II show that the magnitude of R_{ht} is such that the heat flowing in the q_{ht} leg is practically negligible. As a result, a good approximation for the equivalent thermal resistance of the sub-system is simply the sum $R_m + R_r + R_{comb}$. Hence, from Eqs. (I-35) and (I-56),

$$R_{pg} = \frac{T_{pg} - T_\infty}{q_p} = R_m + R_r + R_{comb}$$

$$= \frac{2t - r_g}{2\pi k_p t r_g} + \frac{\ln \frac{r_p}{\sqrt{2/3}\,t} + \frac{k_p}{h r_p}}{2\pi h\left[\frac{k_p}{h}(r_p + t) + \frac{r_p^2}{2} - \frac{t^2}{3}\left(1 + \ln \frac{r_p}{\sqrt{2/3}\,t} + \frac{k_p}{h r_p}\right)\right]} \qquad \text{(I-60)}$$

Because of the geometry of the specimen used as a model for this development, use of the thermal resistance, R_{pg}, from (I-60) is restricted to those installations on flat plates where the gage is mounted near the center of a relatively large surface area.

(b) Under Gage Tab (R_{pt})

Since the gage tab is approximately at the same location on the specimen as the gage grid, the same procedure may be followed to obtain the

resistance of the specimen for heat flow from a gage tab as that developed above for flow from the gage grid. In this manner, with r_t now as the source radius,

$$R_{pt} = \frac{T_{pt} - T_\infty}{q_t} = \frac{2t - r_t}{2\pi k_p t r_t} + R_{comb} \qquad \text{(I-61)}$$

where R_{comb} is identical to that of the previous section and is exhibited as the last term of (I-60). Use of R_{pt} from (I-61) is subject to the same restriction as R_{pg} from (I-60).

APPENDIX II

CALCULATION OF THE COMBINED THERMAL RESISTANCE OF THE HEAT TRANSFER SYSTEM

To determine the magnitude of the thermal resistance of the entire system the individual parameters developed in Appendix I must be evaluated and appropriately combined. These calculations are made herein and lead to approximations which result in a reduced thermal circuit for obtaining the combined thermal resistance. The overall resistance is then calculated from the reduced circuit for the gage-specimen combinations employed experimentally in attempting to determine the validity of this expression for the combined thermal resistance of the system.

A. Strain Gage Properties and Dimensions for use in Calculations

The resistance strain gages used for the experimental verification were manufactured by Micro-Measurements Inc., Romulus, Michigan. The three types selected were the three smallest sizes offered in a series possessing similar grid and tab geometry. Each gage consists of a single constantan etched foil grid mounted on a flexible epoxy backing. No gage covering was utilized. Some pertinent gage properties and dimensions, listed in Table II-1, are used in the calculations that follow. Gage length, as specified in the table, is the length of the grid filaments only. Overall length includes the addition due to the solid loop ends which connect adjacent grid filaments. Overall width includes the gage tabs whereas grid width is the

distance between the outer edges of the outermost grid filaments. Overall gage thickness, by manufacturer's specification, is 0.0012 ± 0.0002 inch and the flexible epoxy film is approximately 0.001 inch thick.

TABLE II-1

STRAIN GAGE DATA

Gage Number	1	2	3
M-M Type	EA-09-015EH -120	EA-09-031EC -120	EA-09-062ED -120
Electrical Resistance, $R_g(\Omega)$	120 ± 0.6	120 ± 0.4	120 ± 0.4
Gage Factor, F	1.98 ± 1%	2.03 ± 1%	2.04 ± 0.5%
Gage Length, ℓ_g(in)	0.015	0.031	0.062
Grid Width, w_g (in)	0.020	0.032	0.063
Overall Length, ℓ_o (in)	0.025	0.042	0.076
Overall Width, w_o (in)	0.100	0.140	0.190
Grid Area, $A_g = \ell_g w_g$ ($in^2 \times 10^{-3}$)	0.300	0.992	3.91
Overall Area, $A_o = \ell_o w_o$ ($in^2 \times 10^{-3}$)	2.50	5.88	14.4
Number of Grid Filaments	17	19	21
Measured Tab Area, A_t ($in^2 \times 10^{-3}$)	0.698	1.64	3.84
Approximate Tab Area, A_t' from Eq.(I-21)($in^2 \times 10^{-3}$)	0.733	1.63	3.50
Equivalent Grid Radius, $r_g = \sqrt{A_g/\pi}$ (in)	0.00977	0.0178	0.0352
Equivalent Tab Radius, $r_t = \sqrt{A_t/\pi}$ (in)	0.0149	0.0228	0.0350

B. Evaluation of Individual Thermal Resistance Parameters

The magnitude of each of these resistances is determined below in the order in which the parameters were developed in Appendix I. To obtain these values the applicable properties and dimensions were inserted into the expressions of Appendix I together with the appropriate constants for compatibility of units.

1. Resistance to Heat Flow From Gage Grid to Tab (R_t)

This parameter is evaluated from

$$R_t = R_g/6\,\rho_g k_g \quad . \qquad \text{(I-14)}$$

Using: R_g = 120 ohms,

ρ_g = 18.5 micro-ohm-inches, and

k_g = 14 BTU/hr-ft-^oF,

then

$$R_t = \frac{12\ (120)}{6(18.5 \times 10^{-6})(14)} = 926{,}000\ \frac{^oF}{BTU/hr} \quad .$$

The value utilized for R_g is the nominal resistance of the gages employed experimentally (Table II-1). That of ρ_g is an average of several values for the electrical resistivity of constantan /36-1130;30-2353,2355; 38-155/ over the temperature range from 20°C to 100°C. That of k_g is also an average of several published values for the thermal conductivity of constantan /36-55,1130;30-2248;9-4.94/ over the same temperature range.

2. Resistance to Heat Flow Through A Lead Wire (R_ℓ)

This resistance is calculated using

$$R_\ell = 1 / \pi r_c \sqrt{2h' k_c r_i} \qquad \text{(I-16)}$$

and

$$h' = \frac{1}{\frac{1}{h} + \frac{r_i \ln (r_i/r_c)}{k_i}} \qquad \text{(I-17)}$$

In some of the early tests AWG #22 solid copper wire with vinyl insulation was used. For this wire the following properties and dimensions apply:

$r_c = 0.0125$ in $\qquad r_i = 0.0215$ in

$k_c = 226$ BTU/hr-ft-°F $\qquad k_i = 0.089$ BTU/hr-ft-°F

where k_c and k_i were obtained from the "Materials Selector" /14-110,197 respectively/. The surface heat transfer coefficient, h, lies in the range between 1 and 5 BTU/hr-ft^2-°F for natural convection /33-15/. Arbitrarily taking h = 2.00 BTU/hr-ft^2-°F

$$h' = \frac{1}{0.500 - \frac{0.0215 \ln (0.0215/0.0125)}{12\,(0.089)}} = 2.01 \ \frac{BTU}{hr\text{-}ft^2\text{-}°F}$$

and

$$R_\ell = \frac{1}{\pi (0.0125/12) \sqrt{2\,(2.01)(226)(0.0215/12)}} = 240 \ \frac{°F}{BTU/hr}$$

As noted in the development of R_ℓ in Appendix I (p. I-6) this value applies only for "infinitely long" leads. For finite leads the correction factor, tanh $m\ell$, must be applied. But, tanh $x \approx 1$ for $x \gtrsim 3$.

and

$$m = \sqrt{h'P/k_c A_c} = (1/r_c) \sqrt{2h' r_i / k_c} = 5.40 \text{ ft}^{-1}.$$

Hence, for this size lead, a length of about 6½ inches is sufficient for the "infinitely long" lead expression to apply. Variations in the properties and dimensions used in calculating m for different leads would require minor adjustments in this length criterion. Therefore, as a general rule, if the lead is approximately one foot or more in length it may be considered "infinitely long" for purposes of this calculation.

For higher values of h in the range specified above, R_ℓ decreases by less than 40%. Also, for AWG #28 copper wire, as used in later tests, R_ℓ would be approximately double that calculated above. Most installations will utilize leads in the range from #28 to #22 gage wire. Then, considering both variations in the surface coefficient and wire size, the value of thermal resistance obtained above is typical for the leads used in connecting strain gages.

3. Resistance to Heat Flow at Exposed Surface

(a) From Gage Tab (R_s)

The resistance to heat flow from an exposed surface is

$$R_s = 1 / hA_t \qquad \text{(I-20)}$$

Using the measured values of tab area from Table II-1 (p. II-2) and surface heat transfer coefficients

in the range specified in the preceding section for this calculation the thermal resistances listed in Table II-2 were obtained.

TABLE II-2

RESISTANCE TO HEAT FLOW FROM EXPOSED SURFACE OF GAGE TAB, $R_s(\frac{^oF}{BTU/hr})$

Gage No.	Surface Heat Transfer Coefficient in BTU/hr-ft^2-^{o}F		
	2.00	3.00	4.00
1	103,000	68,900	51,700
2	43,900	29,200	21,900
3	18,800	12,500	9,390

(b) From Gage Grid (R_a)

Inserting the grid areas specified in Table II-1 and the same surface heat transfer coefficients as for the tab into

$$R_a = 1 / hA_g \qquad (I-22)$$

yields the thermal resistances of the grid surfaces as listed in Table II-3.

TABLE II-3

RESISTANCE TO HEAT FLOW FROM EXPOSED SURFACE OF GAGE GRID $R_a\ (\frac{^oF}{BTU/hr})$

Gage No.	Surface Heat Transfer Coefficient in BTU/hr-ft^2-^{o}F		
	2.00	3.00	4.00
1	240,000	160,000	120,000
2	72,700	48,400	36,300
3	18,500	12,300	9,230

4. Resistance to Heat Flow through Backing Material

(a) Under Gage Tab (R_{bt})

The backing resistance under a tab was determined from

$$R_{bt} = d_b / k_b A_t \quad . \qquad \text{(I-24)}$$

The measured tab areas were taken from Table II-1. From measurements made on many of the gages used it was determined that the foil thickness was approximately 0.0002 inch. Hence, from Section II-A (p. II-1), the backing thickness was 0.001 ± 0.0002 inch. A reasonable value for the thermal conductivity of the epoxy film appears to be 0.115 ± 0.015 BTU/hr-ft-^{o}F /20-16,176;14-13,180/. This value is for non-filled epoxy. The exact composition of the film used by the manufacturer was unknown but for a maximum electrical resistance between gage and specimen it seems reasonable that a non-filled epoxy would be used. Using the properties and dimensions in Eq. (I-24) leads to the following values for backing resistance under a tab:

$R_{bt} = 150 \frac{^{o}F}{BTU/hr}$ for gage #1

$R_{bt} = 63.6 \frac{^{o}F}{BTU/hr}$ for gage #2

$R_{bt} = 22.3 \frac{^{o}F}{BTU/hr}$ for gage #3.

Considering combinations of the extremes of the ranges in backing thickness and thermal conductivity which are possible these thermal resistances have an uncertainty ranging between -29% and +38%.

(b) Under Gage Grid (R_{bg})

The backing resistance under the gage grid was found in the same manner as that under a tab. Substituting the grid area from Table II-1 (p. II-2) and the backing thickness and thermal conductivity as specified for the tab calculations into

$$R_{bg} = d_b / k_b A_g \qquad \text{(I-25)}$$

the thermal resistance of the backing under the grid becomes:

$$R_{bg} = 348 \frac{^{o}F}{BTU/hr} \quad \text{for gage \#1,}$$

$$R_{bg} = 105 \frac{^{o}F}{BTU/hr} \quad \text{for gage \#2,}$$

$$R_{bg} = 26.8 \frac{^{o}F}{BTU/hr} \quad \text{for gage \#3.}$$

The same range of uncertainty applies to the resistance under the grid as that for the resistance under the tab.

5. Resistance to Heat Flow through Bonding Adhesive

(a) The applicable expression for this thermal resistance parameter is

$$R_{ct} = d_a / k_a A_t \qquad \text{(I-26)}$$

As in the case of the backing resistance under the tab, the tab area is obtained from the measured values in Table II-1. Eastman 910 adhesive was used as the bonding agent for all installations tested. The thermal conductivity of this cyanoacrylate cement was not available. However, since a good many of its properties /2;18/ coincide with those of other acrylic plastics /20-16;14-174/, it was assumed that the thermal conductivity would also coincide. Hence, a value of 0.125 ± 0.025 BTU/hr-ft-^{o}F was accepted as being reasonable.

Determination of the adhesive thickness was accomplished by measuring the elevation of the exposed surface of the backing material at each corner of the installed gage with respect to the adjacent specimen surface to the nearest 0.0001 inch with a vernier micrometer and then subtracting the backing thickness. This was done on several specimens for which the same gage application technique had been employed. By this method it was found that the thickness of the cement was 0.0005 ± 0.0003 inch.

Using the properties and dimensions described above in Eq. (I-26) resulted in the following values for the thermal resistance of the adhesive under the tab:

$R_{ct} = 68.8 \frac{^{o}F}{BTU/hr}$ for gage #1,

$R_{ct} = 29.3 \frac{^{o}F}{BTU/hr}$ for gage #2,

$R_{ct} = 12.5 \frac{^{o}F}{BTU/hr}$ for gage #3.

Combining the extreme values of the ranges of adhesive thickness and thermal conductivity leads to an uncertainty range from -66% to +100% for this thermal resistance parameter.

(b) Under Gage Grid (R_{cg})

Inserting the grid area from Table II-1 (p. II-2) and the adhesive thickness and thermal conductivity as described above in the case for the tab into

$$R_{cg} = d_a/k_a A_g \qquad (I-27)$$

resulted in the values for the thermal resistance of the adhesive under the grid listed below:

$R_{cg} = 160 \frac{^{o}F}{BTU/hr}$ for gage #1,

$R_{cg} = 48.4 \frac{^{o}F}{BTU/hr}$ for gage #2,

$R_{cg} = 12.3 \frac{^{o}F}{BTU/hr}$ for gage #3.

As for the resistance of the cement under a tab, the extremes in the uncertainty range for these resistances are -66% and + 100%

6. Resistance to Heat Flow through the Specimen and its Surfaces

(a) Under Gage Grid (R_{pg})

To determine the magnitude of R_{pg} all of the thermal resistance parameters of the

sub-system shown in Fig. I-3 (p. I-13) must be evaluated and combined. These values are determined below in the order in which the parameters were developed in Section 6 (a) of Appendix I.

The resistance of the small hemisphere directly under the gage grid is

$$R_m = 1/2\pi k_p r_g \quad . \qquad \text{(I-30)}$$

The equivalent radii of the grids, r_g, are listed in Table II-1. The gages were attached to specimens of stainless steel in the 300 series and 2024 aluminum. The respective thermal conductivities, k_p, for these materials are 9.4 BTU/hr-ft-°F and 111.0 BTU/hr-ft-°F /14-61,101/. Inserting these values into (I-30) yields the thermal resistances listed in Table II-4.

TABLE II-4

THERMAL RESISTANCE OF SMALL HEMISPHERE UNDER GAGE GRID, $R_m\left(\frac{°F}{BTU/hr}\right)$

Specimen Material	Gage Number		
	1	2	3
Stainless Steel	20.8	11.4	5.78
Aluminum	1.76	0.966	0.489

Appendix I gives the resistance to heat flow through the hollow hemisphere portion of the specimen as

$$R_r = \frac{t - r_3}{2\pi k_p t r_3} = R_m \frac{t - r_3}{t} \qquad (I\text{-}37)$$

The grid radii are again those of Table II-1. The thickness of the specimens used, t, and the corresponding values of R_r are listed below in Table II-5.

TABLE II-5

RESISTANCE TO HEAT FLOW THROUGH HOLLOW HEMISPHERE PORTION OF SPECIMEN, R_r $\left(\frac{^{o}F}{BTU/hr}\right)$

Specimen Material	Specimen Thickness	Gage Number		
		1	2	3
Stainless Steel	0.125"	19.2	9.78	4.14
	0.048"	16.6	7.18	1.54
Aluminum	0.125"	1.62	0.828	0.351
	0.045"	1.38	0.583	0.107

The equivalent thermal resistance of the parallel branches in the q_k leg of Figure I-3 (p. I-13) is given by

$$R_{comb} = \frac{\ln \frac{r_p}{\sqrt{2/3}\, t} + \frac{k_p}{h r_p}}{2\pi h \left[\frac{k_p}{h}(r_p + t) + \frac{r_p^2}{2} - \frac{t^2}{3}\left(1 + \ln \frac{r_p}{\sqrt{2/3}\, t} + \frac{k_p}{h r_p}\right)\right]} \qquad \text{(I-56)}$$

The plate thicknesses, t, and thermal conductivities, k_p, are as previously specified. Taking the surface heat transfer coefficient, h, as 2.00 BTU/hr-ft^2-^{o}F the resulting values of R_{comb} for the various plate sizes are listed below in Table II-6. Variation of the surface heat transfer coefficient within the range specified in Section II-B-2 (p. II-4) results in a range of these resistances from about half to double the values tabulated. However, it will be seen below in the calculations for R_{th} that this variation has little effect on the overall thermal resistance of the system.

TABLE II-6

EQUIVALENT COMBINED THERMAL RESISTANCE OF R_{hb}, R_{fk}, R_e, AND R_{fh}, R_{comb} $(\frac{^oF}{BTU/hr})$

Specimen Material	Specimen Thickness	Specimen Radius		
		3.385"(6"x6")*	2.257"(4"x4")*	1.128"(2"x2")*
Stainless Steel	0.125"	1.13	2.36	8.46
	0.048"	1.21	2.51	9.15
Aluminum	0.125"	0.98	2.16	8.19
	0.045"	1.01	2.24	8.68

*Numbers in parentheses are dimensions of surface of plate employed.

The thermal resistance at the upper surface of the central cylinder portion of the specimen is calculated from

(I-59)

$$R_{ht} = \frac{1}{\pi h\left(\sqrt{\frac{2}{3}}t - r_g\right)\left\{\left(\sqrt{\frac{2}{3}}t + r_g\right) - \left(\sqrt{\frac{2}{3}}t - r_g\right)\left[\frac{1}{1 + (r_g/t)(2\pi k_p t R_{comb} - 1)}\right]\right\}}$$

Considering the gage-specimen combinations used, this expression will have a minimum value for gage #2 mounted on a 2"x2"x$\frac{1}{8}$" aluminum plate with a surface coefficient of 5.00 BTU/hr-ft^2-^{o}F. Under these conditions $R_{ht} = 986 \frac{^oF}{BTU/hr}$. Examination of Tables II-5 and II-6 shows that this value is almost 60 times the resistance of the heat path parallel to R_{ht} in Figure I-3 under corresponding conditions and is about 36

times the sum of the maximum values from each of these tables. This indicates that the heat flow through the R_{ht} branch is negligible compared with that through the parallel branch composed of R_r and R_{comb}. Hence, the assumption involved in the final compilation of R_{pg} in Appendix I (p. I-21) is justified.

The total resistance to heat flow through the specimen and its surfaces under the grid is then determined from

$$R_{pg} = R_m + R_r + R_{comb} \qquad (I-60)$$

where R_m, R_r, and R_{comb} are obtained from Tables II-4, 5, and 6 respectively. These values are listed in Table II-7 for the various combinations of gages and specimens employed experimentally.

Note from Table II-7 that the size of the specimen has relatively little effect on the resistance compared with the effect of the specimen material.

TABLE II-7

THERMAL RESISTANCE OF SPECIMEN UNDER GAGE GRID, $R_{pg}(\frac{^{o}F}{BTU/hr})$

Specimen Material	Specimen Dimensions	Gage Number		
		1	2	3
Stainless Steel	6"x6"x1/8"	41.1	22.3	11.1
	4"x4"x1/8"	42.4	23.5	12.3
	2"x2"x1/8"	48.5	29.6	18.4
	6"x6"x.048"	38.6	19.8	8.5
	4"x4"x.048"	39.9	21.1	9.8
	2"x2"x.048"	46.5	27.7	16.5
Aluminum	6"x6"x1/8"	4.36	2.77	1.82
	4"x4"x1/8"	5.54	3.95	3.00
	2"x2"x1/8"	11.6	9.98	9.03
	6"x6"x.045"	4.15	2.56	1.61
	4"x4"x.045"	5.38	3.79	2.84
	2"x2"x.045"	11.8	10.2	9.28

(b) Under Gage Tab (R_{pt})

The thermal resistance of the specimen under a gage tab may be computed from Eq. (I-61)(p.I-22). This expression is identical to (I-60) from which R_{pg} was obtained above except that the equivalent tab radius, r_t, has been substituted for the equivalent grid radius, r_g. But Table II-1 (p.II-2) shows that r_t and r_g are of the same order of magnitude. Therefore, the values of this resistance parameter, R_{pt}, will have the same order of magnitude as those listed in Table II-7 for the

resistance under the gage grid. Additionally, in determining the overall thermal resistance of the system, R_{th}, in Section II-C below, it will be seen that exact values of R_{pt} are not required. Hence, the order of magnitude values referred to above are sufficiently accurate for the specimen resistance under a gage tab.

C. Combination of the Individual Parameters Forming the Equivalent Thermal Resistance of the System

The total, steady-state, thermal resistance of the system is now obtained by examining the magnitudes of the parameters evaluated in Part II-B above, making various approximations to eliminate several of the parameters based on these relative magnitudes, and then combining the remaining terms analytically. To aid in visualizing the overall effect of the individual resistances Figure 2 (p.10) is repeated here as Figure II-1. The values calculated in Part II-B for these parameters have been inserted in the appropriate blocks of the diagram. Reading down, the numbers in the blocks correspond to Gages 1, 2, and 3, respectively. The specimen resistances under the grid, R_{pg}, as shown are averages of those listed in Table II-7 for the various specimen sizes corresponding to a given gage size and specimen composition. The values of R_{pt} shown are identical to those of R_{pg} since, as previously

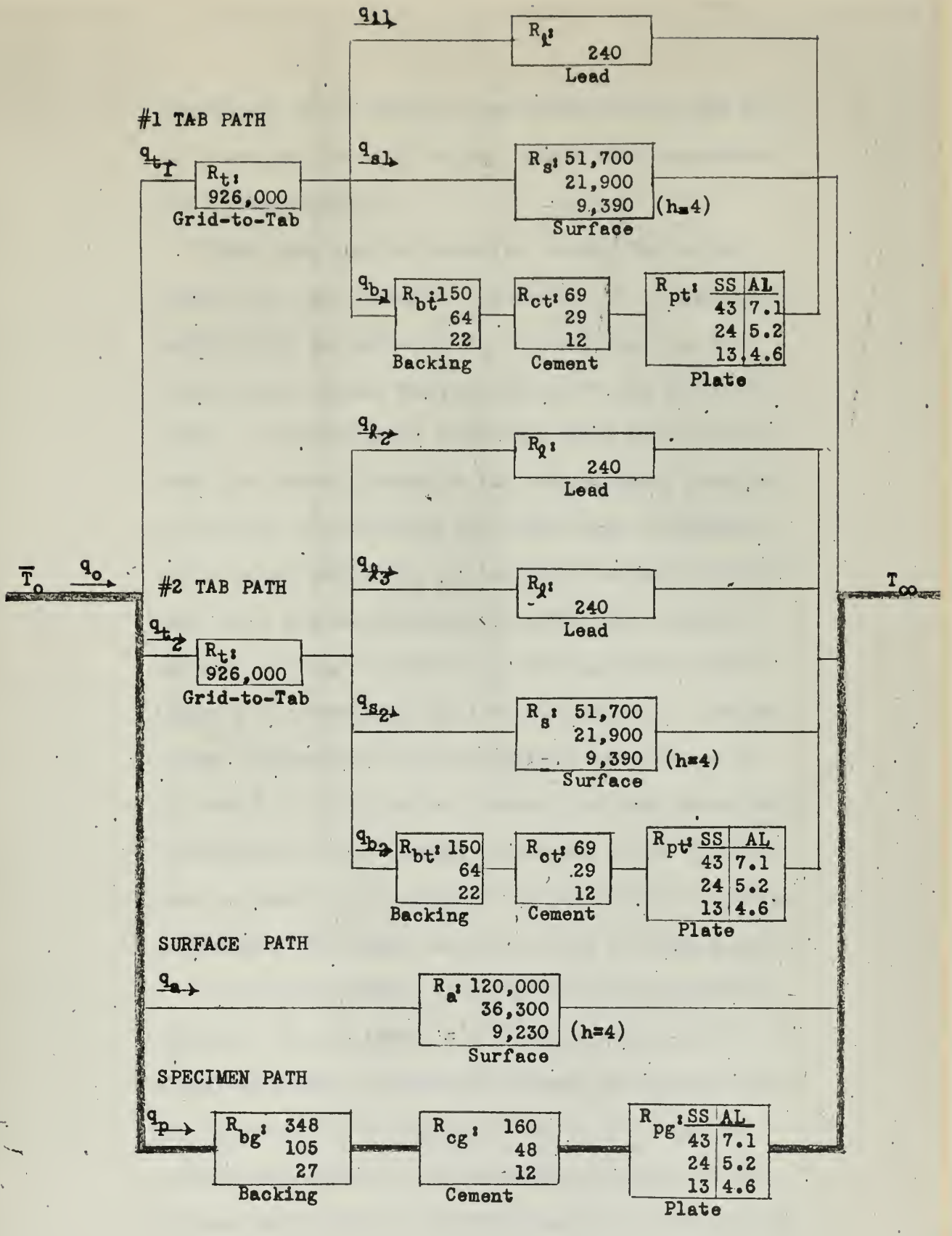

FIG. II-1

SCHEMATIC DIAGRAM OF STEADY STATE HEAT TRANSFER SYSTEM WITH PARAMETERS EVALUATE
Numbers reading down are for gages one, two and three respectively in ^{o}F-hr/BTU.
R_{pt} and R_{pg} are averages for the various specimen sizes.

determined, their orders of magnitude are the same and, as is evident from the diagram, their exact magnitudes are inconsequential.

Upon examining the parallel combination in the upper right hand corner of Figure II-1 it is immediately evident that the values of R_s in the center leg are exceptionally larger than the values in the other two legs. It can easily be shown that these values are at least 200 times as large as the corresponding parallel equivalents for the upper and lower legs. Therefore, in all practicality, R_s can be treated as being infinitely large and be eliminated from the heat transfer circuit. Having eliminated R_s, the equivalent resistance of the remaining parallel combination is insignificant compared with the extremely large value of R_t with which it is in series. Hence, the only appreciable contribution to the thermal resistance of the first tab path is that from the grid to the tab itself. A similar analysis of the second tab path yields the same result.

In the development of the grid-to-tab resistance parameter, R_t, in Appendix I it was assumed that the effect of thermal interaction between grid filaments was negligible for this application (p. I-4). From the relative magnitudes of the parameters involved it may be seen that even if this effect would reduce R_t by 90%, which is unlikely, the ratio of R_t to the resistance of the parallel combination in series with it would still be about 1000:1.

Another assumption in the development of R_t (p.I-3) was that $T_t \simeq T_\infty$. Since the temperature drop along the path is proportional to the resistance of the path it is evident from the previous paragraph that the temperature drop from the tab to ambient is less than 1/1000 of the total drop. Thus, as an example, for a temperature difference of 500°F between the grid and ambient the drop from the tab to ambient would be less than $\frac{1}{2}$°F. Hence, this assumption is also justified.

Also note from the above analysis that the leads have a negligible effect on the heat transfer mechanism. Thus, as asserted in the development of the lead resistance, R_ℓ (p. I-6), the details of local conditions at the lead-tab junction are insignificant.

Having reduced each of the two tab paths to the single value of R_t the circuit of Fig. II-1 can now be further reduced.

For the values tabulated on the diagram it can be shown that, for a given gage, the equivalent resistance of the upper three parallel paths (the two tab paths and the surface path) is at least 174 times the sum of the resistances in the specimen path. Even considering the case where the adverse extremes of the ranges of these resistance parameters occur together the ratio of the parallel equivalent resistance of the upper three paths to the series equivalent resistance of the lower path is about 40:1. These ratios are sufficiently

large that, for practical applications, the parallel combination of R_t, R_t , and R_a may now be considered as an infinitely large resistance. Hence, the two tab paths and the surface path may be eliminated from the analogue circuit.

The remaining portion of the schematic diagram is indicated by the heavy line in Figure II-1. This line shows appreciable heat flow through the specimen path only. Thus, the parameters which resist heat flow from the gage grid through the gage backing, R_{bg}; through the bonding adhesive, R_{cg}; and through the specimen and its surfaces, R_{pg}, to the atmosphere are the primary ones affecting overall thermal resistance of the system, R_{th}. Therefore,

$$R_{th} = (\bar{T}_o - T_\infty)/q_o = R_{bg} + R_{cg} + R_{pg} \quad . \qquad (II-1)$$

Using the values for R_{cg}, R_{bg}, and R_{pg} computed in Section II-B, the total thermal resistance of the system for each of the various test combinations is as listed below in Table II-8. Considering combinations of the extremes of the ranges in all of the properties and dimensions and the accuracy of the approximations employed in calculating these tabulated values of R_{th} it is estimated that an uncertainty ranging between -40% and +55% should be associated with each value.

Using the parametric expressions for R_{bg}, R_{cg}, and R_{pg} from Eqs. (I-25), (I-27), and (I-60) respectively, the total thermal resistance of the system may be expressed as

$$R_{th} = \frac{1}{A_g}\left[\frac{d_b}{k_b} + \frac{d_a}{k_a}\right] + \frac{2t - \sqrt{A_g/\pi}}{2k_p t\sqrt{\pi A_g}}$$

$$+ \frac{\ln\frac{r_p}{\sqrt{2/3}\,t} + \frac{k_p}{h r_p}}{2\pi h\left[\frac{k_p}{h}(r_p + t) + \frac{r_p^2}{2} - \frac{t^2}{3}\left(1 + \ln\frac{r_p}{\sqrt{2/3}\,t} + \frac{k_p}{h r_p}\right)\right]} \qquad \text{(II-2)}$$

TABLE II-8

COMBINED THERMAL RESISTANCE OF ENTIRE HEAT TRANSFER SYSTEM,

R_{th} $\left(\frac{^{o}F}{BTU/hr}\right)$

Specimen Material	Specimen Dimensions	Gage Number / Grid Areas ($in^2 x10^{-3}$)		
		1/0.300	2/0.992	3/3.90
Stainless Steel	6"x6"x1/8"	550	180	50
	4"x4"x1/8"	550	180	51
	2"x2"x1/8"	560	180	57
	6"x6"x.048"	550	170	48
	4"x4"x.048"	550	170	49
	2"x2"x.048"	550	180	56
Aluminum	6"x6"x1/8"	510	160	41
	4"x4"x1/8"	510	160	42
	2"x2"x1/8"	520	160	48
	6"x6"x.045"	510	160	41
	4"x4"x.045"	510	160	42
	2"x2"x.045"	520	160	48

APPENDIX III

EXPERIMENTAL RESULTS

The specific experiments performed in accordance with the procedures described in Section 3 are discussed in detail in this appendix. Values of the various parameters determined from these tests as well as the status of the test variables for each run are tabulated at the end of this section.

The fractional changes in the electrical resistance of the gage due to elevated oven temperatures for several of the uniform heating cycles are listed in Table III-1 (p. III-6). The tabulated values of resistance change show relatively minor variations about zero for the gages attached to the stainless steel plates except for the first cycle of gage 1A where a great deal of hysteresis was evident. These trends indicate the effectiveness of the self-temperature-compensation characteristics of the gages. Those gages attached to aluminum plates show an increasing positive resistance change with increasing temperature.

The theoretical temperature coefficient of resistance for the case of uniform heating of a self-temperature-compensated gage installation is given by Eqs. (9) and (11) (p. 7) as

$$\eta' = F(\alpha_p - \alpha_c) \quad . \qquad \text{(III-1)}$$

In applying this expression to the gage 1A - stainless steel specimen combination it is seen that η' is zero because the gage is compensated for the material to which it is attached. That is, the thermal coefficients of expansion for the specimen and

the material for which the gage is compensated are the same. For an aluminum specimen, however, this result would not be zero since the expansion coefficients are different. Using coefficients of 9.6×10^{-6} / °F and 12.6×10^{-6} / °F respectively for the stainless steel and aluminum and the gage factor (1.98) provided by the manufacturer for gage #1 it is predicted by (III-1) that the thermal coefficient of resistance of the system for this case is about 6 $\frac{\mu\Omega}{\Omega}$ per °F. As before, the material properties used are averages of the values listed in several publications and may vary by about ± 10%.

The results of the several attempts at verification of the thermal resistance of the system by the temperature measurement method are listed in Table III-2 (p. III-7). These tests were all performed on 6"x6"x1/8" stainless steel specimens.

Runs 1 through 4 employed the iron-constantan thermocouples with integral leads. In Runs 1 and 2 the junctions were varnish coated and mounted vertically. Both provided almost identical results as seen from the tabulated values. For Run 3 the varnish coated Fe-Cn thermocouple was mounted horizontally and thermally insulated from the environment as described in Section 3. This scheme was expected to produce higher junction temperatures than the previous cases. But, as is obvious from the tabulation, the resulting measured temperatures were lower. This result is attributed to a greater contact resistance between the thermocouple and the gage grid due to the lower pressure applied. Run 4 utilized the Sauereisen #29 coated junction mounted vertically.

The results, as listed, are seen to be about the same as those of Run 3. Again, high contact resistance is deemed to be the cause due, this time, to the greater surface roughness of the Sauereisen cement.

The varnish coated, micro-miniature, copper-constantan thermocouple junction was used for Runs 5 through 12. Runs 5 and 8 for gage 2A employed 0.020" and 0.010" diameter leads respectively. It was expected from the calculation discussed in Section 3 (p.24) that both runs would yield the same results. However, Run 8 with the smaller leads provided appreciably lower temperatures as seen by the values listed in Table III-2. The difference can only be attributed to greater contact resistance as before. Run 12 utilized the same apparatus as Run 7 (gage 1A and 0.010" diameter thermocouple leads) but was performed after four intervening uniform heating cycles in the oven. The large increase in measured temperatures shown may be partially due to a better bond between gage and specimen resulting from adhesive curing but is more probably due to better physical contact between the thermocouple junction and the gage grid. The fact that Run 6 (0.020" leads) resulted in approximately the same values as 12 is merely coincidental. It was found that the electrical resistance between thermocouple and gage was only about 75 ohms for Run 6. Hence, an appreciable leakage path for gage current was established and the normal system performance was extensively disrupted.

The method for determining the equivalent thermal resistance of the system by measuring the electrical resistance changes of

the strain gage provided the results listed in Table III-2 (for Runs 7, 8, and 12) and III-3. The tabulated values were obtained by the procedure described in Section 3. The applicable variables for each test performed are also listed in the tables. In addition, the slope of the linear portion of the curve from a plot of the fractional change of electrical resistance of the gage as a function of the power dissipated by the gage was obtained for each run. Theoretically, this slope is the product of the temperature coefficient of electrical resistance and the equivalent thermal resistance of the system as shown by Eq. (18):

$$\frac{\Delta R_g / R_g}{I_g^2 R_g} = \eta R_{th} .$$

The slope obtained as above was divided by η from Eq. (12)(p. 8) to provide the experimentally determined value of R_{th} listed in Tables III-2 and III-3. For comparison purposes the corresponding calculated value of R_{th} from Table II-8 (p. II-22) is also tabulated for each run.

In general, all of the tests made using the resistance measuring technique were performed in the same manner with the same apparatus. However, minor variations in equipment and procedure were employed to show the effect of specific operating conditions on system performance in some of the experiments. These are discussed below.

To demonstrate the negligible heat dissipation through the lead wires Runs 12 and 13 were performed with the same gage-specimen combination but with different leads. In Run 12 AWG #22 (0.025" diameter) solid copper leads were employed. AWG #28

(0.0126" equivalent wire diameter) stranded copper wires were used for Run 13. Both tests were made using the three-wire gage connection circuit. This circuit compensated any lead wire resistance changes due to temperature variations but did not prevent heat dissipation through the leads.

A further indication of the lead wire effects was shown by Runs 41 and 42. These tests were made using the same gage on the same specimen and with the same size leads (AWG #28 stranded copper) but in different circuits. Run 41 employed the three-wire scheme as above. In Run 42 the standard two-wire bridge connection was used. If any temperature variation occurred in the leads its effect would be easily observed by comparing the results of these two runs.

The relative significance of the heat dissipated from the exposed surfaces of the gage grid and tabs was shown by Runs 22 and 23. These tests were based on the principle that the amount of heat convected from a hot surface facing upward is different than that from a hot surface facing downward /33-311/. Run 22 was performed with the gage on the upper surface of the plate as in the general case. The specimen plate was then turned over and Run 23 was made with the gage on the bottom. Any appreciable difference between the results of these two experiments may be attributed to the heat dissipation from the exposed surfaces.

Discussion and evaluation of the experimental results presented in the following tables will be found in Section 4.

TABLE III-1

FRACTIONAL RESISTANCE CHANGE OF GAGE AT UNIFORM ELEVATED TEMPERATURE

Gage Number	1A		1A		1C		1D		2B		2C	
Grid Area, A_g ($in^2 \times 10^{-3}$)	0.30		0.30		0.30		0.30		0.99		0.99	
Run Number	9		10		15		34		30		32	
Plate Material	SS		SS		Al		Al		SS		SS	
Plate Thickness	1/8"		1/8"		1/8"		0.045"		1/8"		0.048"	
Surface Dimensions	6"x6"		6"x6"		6"x6"		6"x6"		6"x6"		4"x4"	
Oven Cycle Number	1		3		5		5		5		5	
Lead Wires AWG	22		22		28		28		28		28	
	T (^oF)	$\Delta R_g/R_g$ ($\mu\Omega/\Omega$)	T (^oF)	$\Delta R_g/R_g$ ($\mu\Omega/\Omega$)	T (^oF)	$\Delta R_g/R_g$ ($\mu\Omega/\Omega$)	T (^oF)	$\Delta R_g/R_g$ ($\mu\Omega/\Omega$)	T (^oF)	$\Delta R_g/R_g$ ($\mu\Omega/\Omega$)	T (^oF)	$\Delta R_g/R_g$ ($\mu\Omega/\Omega$)
	71	0	72	0	72	0	72	0	71	0	72	0
	85	-7.0	84	-13	83	28	85	101	87	-28	87	-18
	100	-7.0	94	-13	96	80	96	155	94	-34	96	-22
	116	-76	114	37	113	141	112	259	110	-50	113	-49
	131	-267	132	47	127	206	128	369	125	-70	128	-63
	146	-612	145	13	148	319	145	549	141	-97	146	-90
	170	-2038	163	-46	164	413	167	620	164	-57	164	-63

TABLE III-2

THERMOCOUPLE TEMPERATURE RISE AT VARIOUS GAGE POWER LEVELS
(Including Fractional Resistance Change for Runs 7, 8, and 12)

Run Number*	1	2	3	4	5	6	7	8	12
Gage Number	2A	2A	2A	2A	2A	1A	1A	2A	1A
Grid Area, A_g ($in^2 x 10^{-3}$)	0.99	0.99	0.99	0.99	0.99	0.30	0.30	0.99	0.30
R_{th}, Calculated $\frac{^oF}{BTU/hr}$	180	180	180	180	180	550	550	180	550
η, Calculated $\frac{\mu\Omega}{\Omega}$ /^oF	-19.5	-19.5	-19.5	-19.5	-19.5	-19.0	-19.0	-19.5	-19.0
R_{th}, Experimental, Temp. ($\frac{^oF}{BTU/hr}$)	30	30	20	20	70	180	80	60	180
R_{th}, Experimental, Resis. ($\frac{^oF}{BTU/hr}$)	--	--	--	--	--	--	305	147	244

q_o ($\frac{BTU}{hr} x 10^{-3}$)	q_o (mW)	I_g (ma)	V_b (v)	ΔT (^oF)	ΔT (^oF)	ΔT (^oF)	ΔT (^oF)	ΔT (^oF)	ΔT (^oF)	ΔT (^oF)	$\Delta R_g/R_g$ ($\frac{\mu\Omega}{\Omega}$)	ΔT (^oF)	$\Delta R_g/R_g$ ($\frac{\mu\Omega}{\Omega}$)	ΔT (^oF)	$\Delta R_g/R_g$ ($\frac{\mu\Omega}{\Omega}$)
1.64	0.48	2	1.04	0	0	0	0	0	0	1	0	0	0	0	0
10.2	3.00	5	2.60	0	0	0	1	1	1	1	-89	0	-44	1	-76
41.0	12.0	10	5.20	1	1	0	1	3	5	4	-267	0	-151	6	-186
92.1	27.0	15	7.80	2	3	1	2	6	12	8	-578	4	-304	14	-407
164.0	48.0	20	10.4	6	5	3	4	12	30	13	-971	8	-517	27	-718
256.0	75.0	25	13.0	9	9	5	6	18	48	20	-1517	14	-766	44	-1090
369.0	108.0	30	15.6	12	12	7	8	25	64	28	-1918	19	-1017	61	-1352
502.0	147.0	35	18.2	18	18	11	10	35	90	40	-2435	28	-1360	89	-1501
655.0	192.0	40	20.8	23	24	14	14	46	116	54	-2550	38	-1682	118	-1304
829.0	243.0	45	23.4	32	31	19	18	60	152	76	-1716	52	-2010	--	--
1024.0	300.0	50	26.0	40	40	24	22	74	--	95	-692	65	-2160	--	--

*All on 6"x6"x1/8" SS, AWG #22 leads

TABLE III-3

FRACTIONAL RESISTANCE CHANGE AT VARIOUS GAGE POWER LEVELS

Gage Number				1A	1C	1C		1D	1D	1D	3B	3B
Grid Area, A_g ($in^2 x10^{-3}$)				0.30	0.30	0.30		0.30	0.30	0.30	3.9	3.9
Run Number				13	16	19		35	38	39	41	42
Plate Material				SS	Al	Al		Al	Al	Al	SS	SS
Plate Thickness				1/8"	1/8"	1/8"		.045"	.045"	.045"	1/8"	1/8"
Plate Surface				6"x6"	6"x6"	4"x4"		6"x6"	4"x4"	2"x2"	6"x6"	6"x6"
Prior Oven Cycles				4	5	5		5	5	5	4	4
Lead Wire Gage No.				28	28	28		28	28	28	28	28
R_{th}, Calculated ($\frac{^oF}{BTU/hr}$)				550	510	510		510	510	520	50	50
η, Calculated ($\frac{\mu\Omega}{\Omega}/^oF$)				-19.0	-19.0	-19.0		-19.0	-19.0	-19.0	-19.6	-19.6
R_{th}, Experimental ($\frac{^oF}{BTU/hr}$)				224	284	278		390	402	399	39.8	39.8
q_o ($\frac{BTU}{hr} X10^{-3}$)	q_o (m W)	I_g (ma)	V (v)	$\Delta R_g/R_g$ ($\frac{\mu\Omega}{\Omega}$)								
1.64	0.48	2	1.04	0	0	0		0	0	0	0	0
10.2	3.00	5	2.60	-36	-37	-40		-65	-61	-53	-11	-25
41.0	12.0	10	5.20	-163	-210	-214		-286	-299	-294	-36	-50
92.1	27.0	15	7.80	-417	-498	-498		-659	-700	-689	-77	-86
164	48.0	20	10.4	-713	-888	-891		-1188	-1232	-1224	-133	-141
256	75.0	25	13.0	-1080	-1347	-1330		-1865	-1894	-1853	-204	-208

TABLE III-3 (Con't.)

Gage Number				2B	2B	2B	2B	2C	2C	2C	2C	2D	2D
Grid Area, A_g ($in^2 x10^{-3}$)				0.99	0.99	0.99	0.99	0.99	0.99	0.99	0.99	0.99	0.99
Run Number				17	31	36	40	22	23	33	37	25	28
Plate Material				SS	SS	SS	SS	SS	SS	SS	SS	A1	A1
Plate Thickness				1/8"	1/8"	1/8"	1/8"	.048"	.048"	.048"	.048"	.045"	.045"
Plate Surface				6"x6"	6"x6"	4"x4"	2"x2"	6"x6"	6"x6"	4"x4"	2"x2"	4"x4"	2"x2"
Prior Oven Cycles				0	5	6	6	2	2	5	5	2	2
Lead Wire Gage No.				28	28	28	28	28	28	28	28	28	28
R_{th}, Calculated ($\frac{^oF}{BTU/hr}$)				180	180	180	180	170	170	170	180	160	160
η , Calculated ($\frac{\mu\Omega}{\Omega}$ /^oF)				-19.5	-19.5	-19.5	-19.5	-19.5	-19.5	-19.5	-19.5	-19.5	-19.5
R_{th}, Experimental ($\frac{^oF}{BTU/hr}$)				201	204	214	215	156	158	155	158	106	106
q_o ($\frac{BTU}{hr}$ $x10^{-3}$)	q_o (m W)	I_g (ma)	V (v)	$\Delta R_g/R_g$ in $\mu\Omega/\Omega$									
1.64	0.48	2	1.04	0	0	0	0	0	0	0	0	0	0
10.2	3.00	5	2.60	-32	-10	-26	-50	-35	-17	-35	-31	-14	-25
41.0	12.0	10	5.20	-153	-124	-163	-178	-123	-113	-124	-120	-72	-81
92.1	27.0	15	7.80	-360	-335	-374	-395	-280	-261	-278	-269	-179	-190
164.0	48.0	20	10.4	-636	-636	-680	-707	-495	-489	-499	-480	-332	-342
256.0	75.0	25	13.0	-1000	-1021	-1051	-1087	-783	-772	-779	-770	-520	-531

thesH2962
Some self-heating characteristics of ver
3 2768 002 07763 8
DUDLEY KNOX LIBRARY